Narcissistic Assembly of Homochiral Covalent Organic Cages with Dehydrobenzo[12]Annulene (DBA) Panels

Carson E. Ward[a], Ryan J. Maguire,[a] Nitesh Kumar,[a] Christopher M. Hadad,[a] and Jovica D. Badjić*[a]

[a] C. E. Ward, R. J. Maguire, N. Kumar, Prof. C. M. Hadad, Prof. J. D. Badjić

Department of Chemistry and Biochemistry

The Ohio State University

100 West 18th Avenue, Columbus, OH 43210 (USA)

E-mail:badjic.1@osu.edu

Supporting Information

General Information

All chemicals were purchased from commercial sources and used as received unless stated otherwise. All solvents were dried before use according to standard literature procedures. Chromatographic purifications were performed with silica gel 60 (SiO_2, 40–75 μm, 200 × 400 mesh). Thin-layer chromatography was performed on a silica gel plate w/UV254 (200 μm). Chromatograms were visualized by UV light or stained with iodine (I_2). All NMR experiments were performed with Bruker 400, 600, and 850 MHz spectrometers. Deuterated solvents $CDCl_3$, $(CD_3)_2SO$ and C_6D_6 were acquired from Cambridge Isotope Laboratories. NMR data was processed and analyzed using Bruker software (Topspin 4.2, Dynamics center 2.8, MestReNova 13.3.3). High-resolution mass data (HRMS) were obtained using electrospray ionization (ESI) techniques (Bruker ESI TOF and Thermo-fisher ESI orbitrap instruments), trapped ion mobility (Bruker TIMS-TOF) and MALDI-MS data (Bruker MALDI-TOF). UV-Vis spectra were recorded with Shimadzu UV-2401PC spectrophotometer using a 1x1 cm quartz cuvette. Circular Dichroism spectra were recorded with JASCO J-1500 using a 1x1 cm quartz cuvette.

Syntheses, Dynamic Imine Condensations, and Characterizations

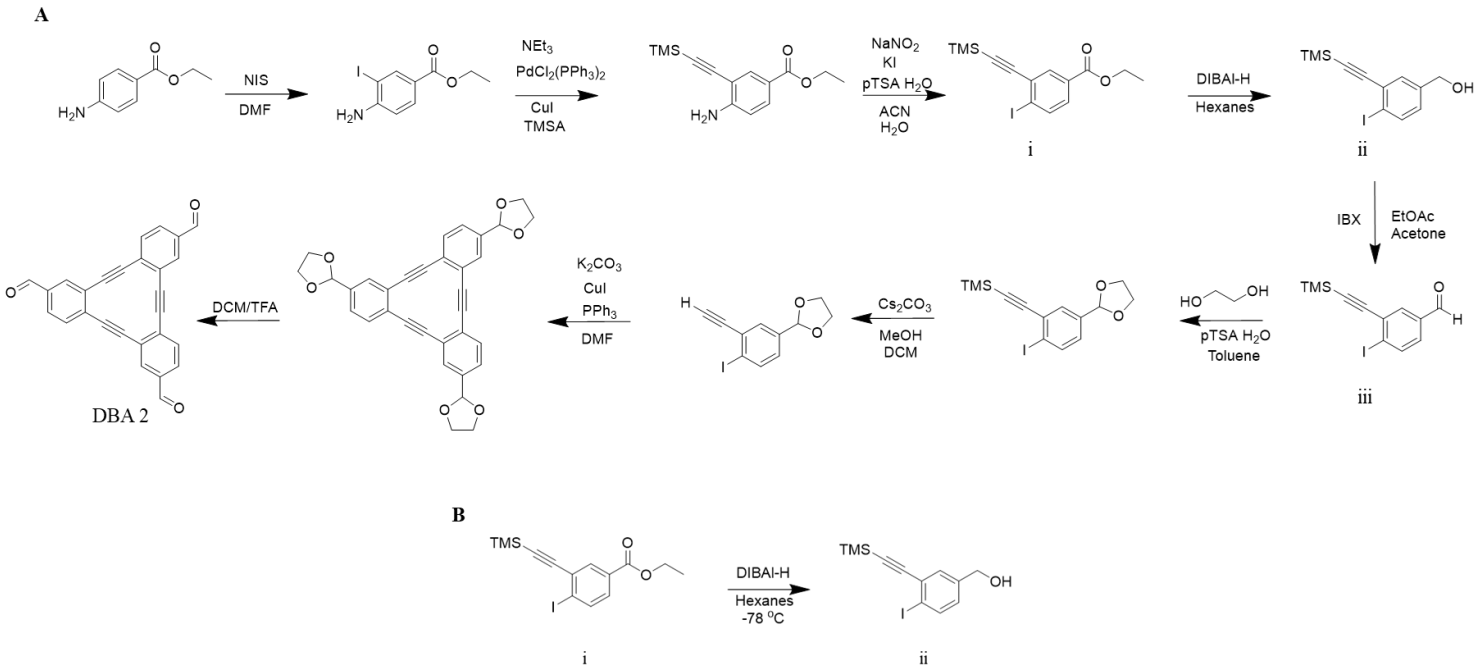

Scheme S1. (A) Synthesis of DBA **2** was completed following method described by McGrier and coworkers in *Mol. Syst. Des. Eng.,* **2020**, 5, 97-101. (B) Reduction of benzoic ester derivative **i** to benzyl alcohol derivative **ii**.

Compound ii: A solution of **i** (4.30 g, 11.55 mmol) in hexanes (25 mL, 0.17 M) was cooled to -78 °C. Meanwhile, a separate vial containing diisobutylaluminum hydride (25 mL, 1M in hexanes; DIBAL-H) was cooled to -78 °C. After cooling for 10 min, DIBAL-H was added dropwise to the solution containing **i** over 30 minutes. The reaction was stirred at -78°C for one hour before the addition of methanol (25 mL) to quench the reaction. This reaction mixture was stirred for an additional 15 min, after which 10 mL of 1 M solution of potassium sodium tartrate tetrahydrate (i.e., Rochelle salt) was added and the mixture was allowed to stir for another hour. After warming back to room temperature, the layers were separated, and the aqueous layer was extracted with hexanes (3 x 15 mL). The organic layers were combined and washed with brine (1 x 30 mL) and

dried over Na_2SO_4. After removing solvent under reduced pressure, the residue was purified by column chromatography (SiO_2, hexanes : ethyl acetate = 3 : 1), yielding **ii** as a dark yellow oil (1.62 g, 42%). ^{1}H NMR (400 MHz, $CDCl_3$) δ (ppm) 7.79 (d, J = 8.23 Hz, 1H), 7.45 (d, J =2.10 Hz, 1H), 6.98 (dd, J = 8.28 Hz, 1H), 4.59 (s, 2H), 0.28 (s, 9H). ^{13}C NMR (100 MHz, $CDCl_3$): δ (ppm) 140.9, 138.9, 131.1, 129.8, 128.1, 106.4, 99.8, 99.0, 64.2, -0.07. HRMS (ESI-MS) m/z calculated for $C_{12}H_{15}IOSi$ $[M+H]^+$: 331.0015; found: 331.0010.

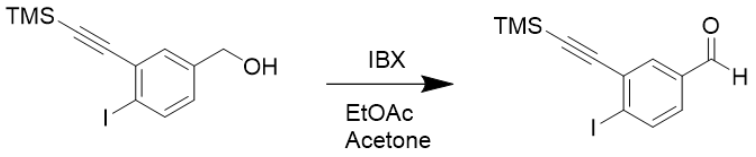

ii iii

Scheme S2. The oxidation of benzyl alcohol derivative **ii** to benzaldehyde derivative **iii** (see Scheme 1).

Compound iii: To a solution of **ii** (1.60 g, 4.84 mmol) in EtOAc (45 mL) and acetone (4.5 mL) was added 2-iodoxybenzoic acid (6.78 g, 24.22 mmol; IBX). The reaction was heated to 90°C for 3 h. After cooling to room temperature, the mixture was filtered through a cotton plug. To the filtrate was added saturated sodium bicarbonate (20 mL), the layers were separated, and the aqueous layer was extracted with ethyl acetate (2 x 15 mL). Combined organic layers were washed with brine (1 x 15 mL) and dried over Na_2SO_4. The residue was concentrated in vacuo and purified by column chromatography (SiO_2, hexanes : ethyl acetate = 2 : 1) to yield compound **iii** as a light-yellow oil (1.55 g, 96%). ^{1}H NMR (400 MHz, $CDCl_3$) δ (ppm) 9.93 (s, 1H), 8.04 (d, J = 8.20 Hz, 1H), 7.91 (d, J = 2.15 Hz, 1H), 7.46 (dd, J = 8.16 Hz, 1H), 0.30 (s, 9H). ^{13}C NMR (100 MHz, $CDCl_3$): δ (ppm) 191.0, 140.0, 136.1, 133.9, 131.3, 129.2, 109.6, 105.4, 101.2, 0.00. HRMS (ESI-MS) m/z calculated for $C_{12}H_{13}IOSi$ $[M+H]^+$: 328.9859; found: 329.0052.

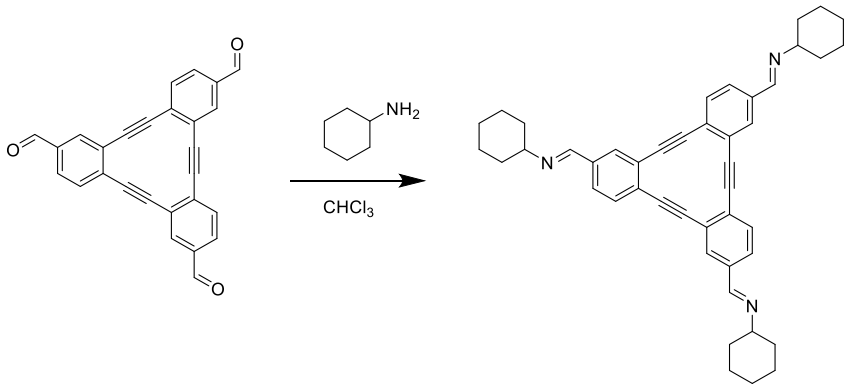

2 4

Scheme S3. Synthesis of model compound **4**.

Compound 4: To a solution of DBA **2** (10 mg, 26 μmol) in $CHCl_3$ (5 mL) was added cyclohexylamine (7.74 mg, 78 μmol). The reaction was stirred at 25 °C for 24 h. After, the mixture was filtered through a cotton plug and solvent removed in vacuo. To the solid was added methanol (5 mL) and sonicated for 60 seconds, then placed in the centrifuge for 5 minutes at 6000 rpm. The liquid was removed to give compound **4** as a light-yellow solid (12.5 mg, 76%). ^{1}H NMR (400 MHz, DMSO-d_6): δ (ppm) 8.36 (s, 1H), 7.80 (d, J = 4 Hz, 1H), 7.69 (dd, J = 8 Hz, 1H), 7.58 (d, J = 8 Hz, 1H), 3.27-3.24 (m, 1H), 1.80-1.78 (m, 2H), 1.70-1.64 (m, 4H), 1.53-1.44 (m, 2H), 1.41-1.31 (m, 2H). ^{13}C NMR (214 MHz, DMSO-d_6) δ (ppm): 157.43, 137.62, 133.12, 131.41, 129.33, 127.29, 126.12, 94.13, 93.15, 69.02, 34.46, 25.69, 24.55. MALDI-TOF (DCTB, reflector mode): m/z calculated for $C_{45}H_{45}N_3$ $[M+H]^+$ 628.369, found: 628.159 (Figure S7).

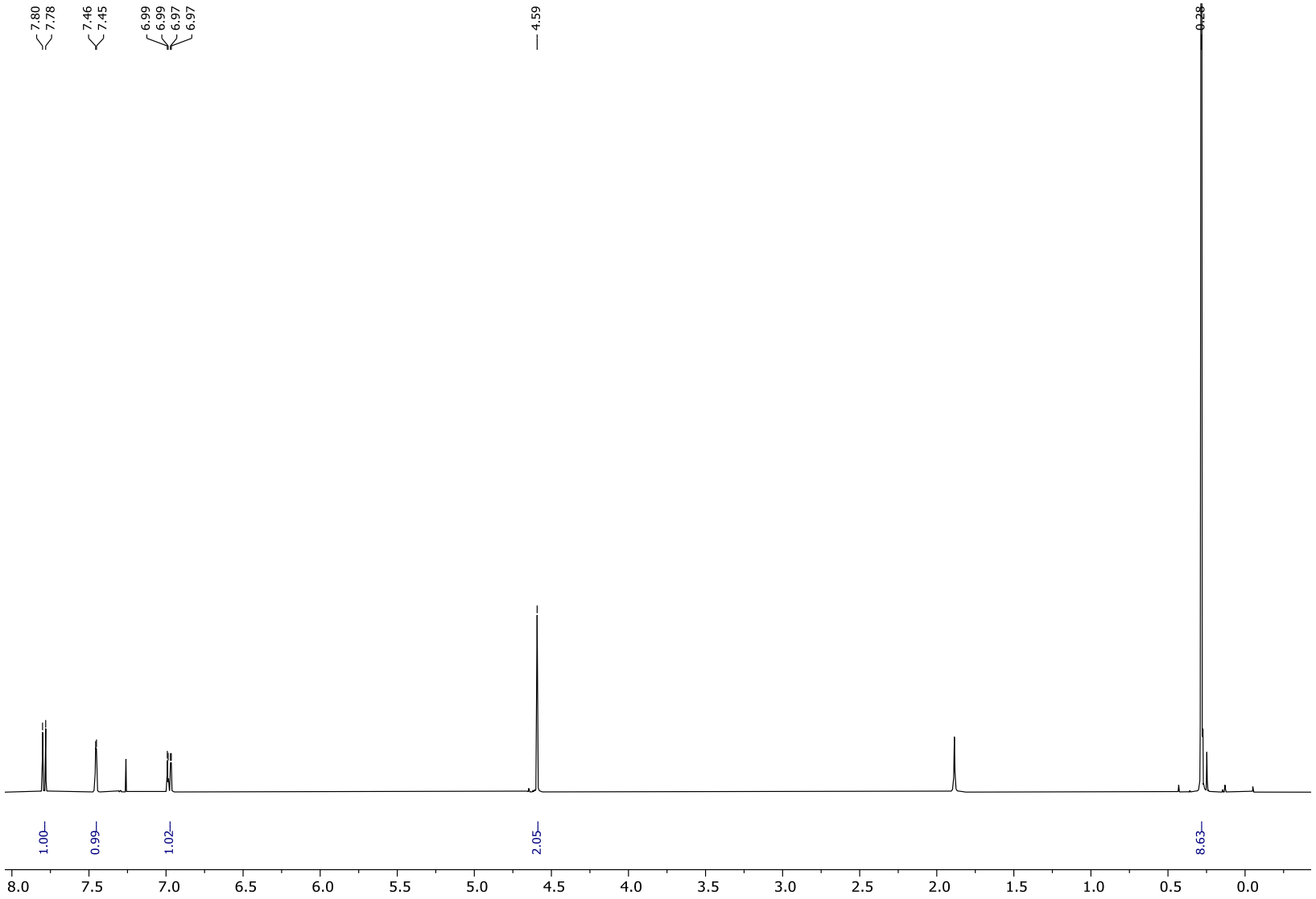

Figure S1. ^{1}H NMR spectrum (400 MHz, 298 K) of compound **ii** in $CDCl_3$.

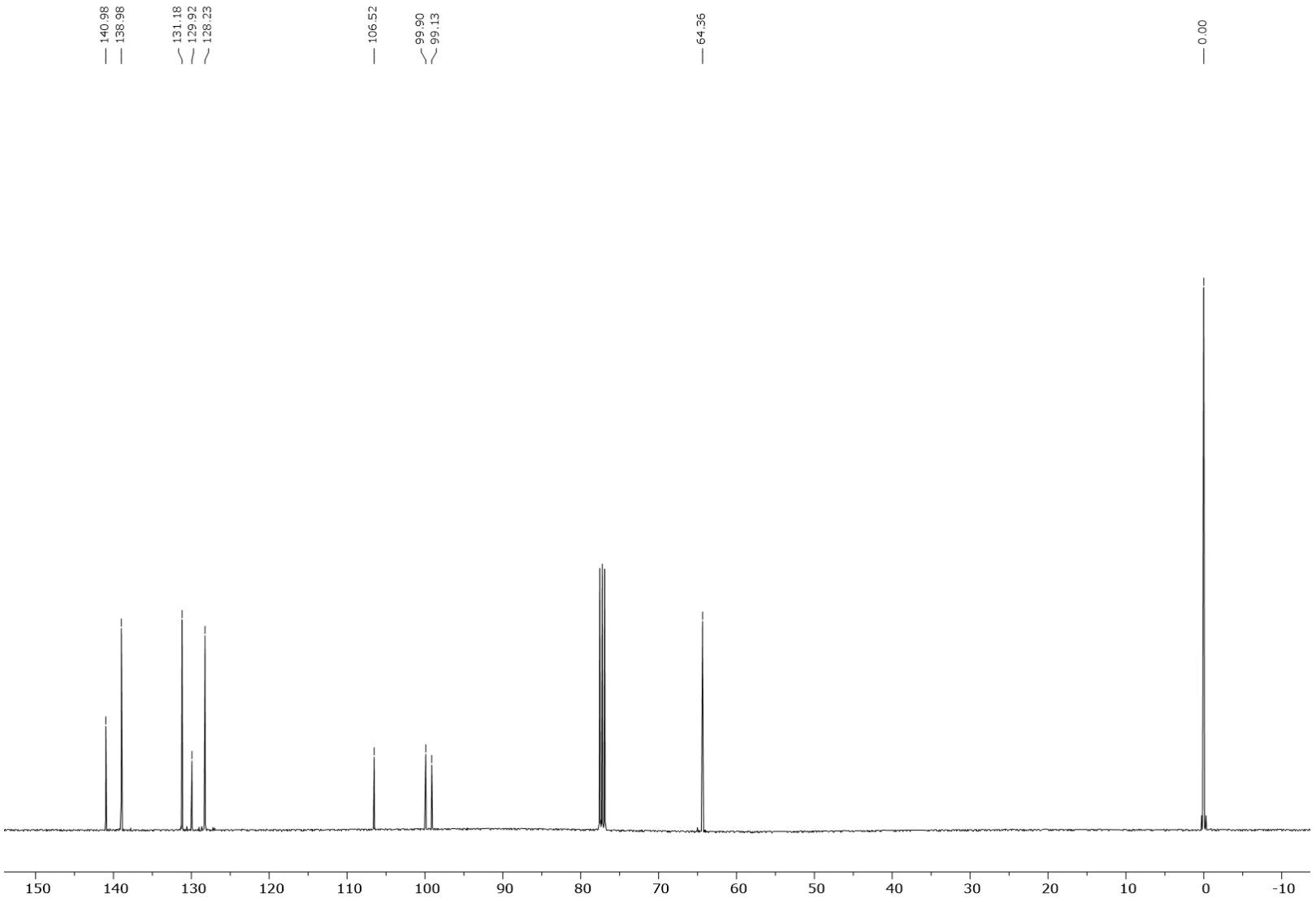

Figure S2. ^{13}C NMR spectrum (100 MHz, 298 K) of compound **ii** in $CDCl_3$.

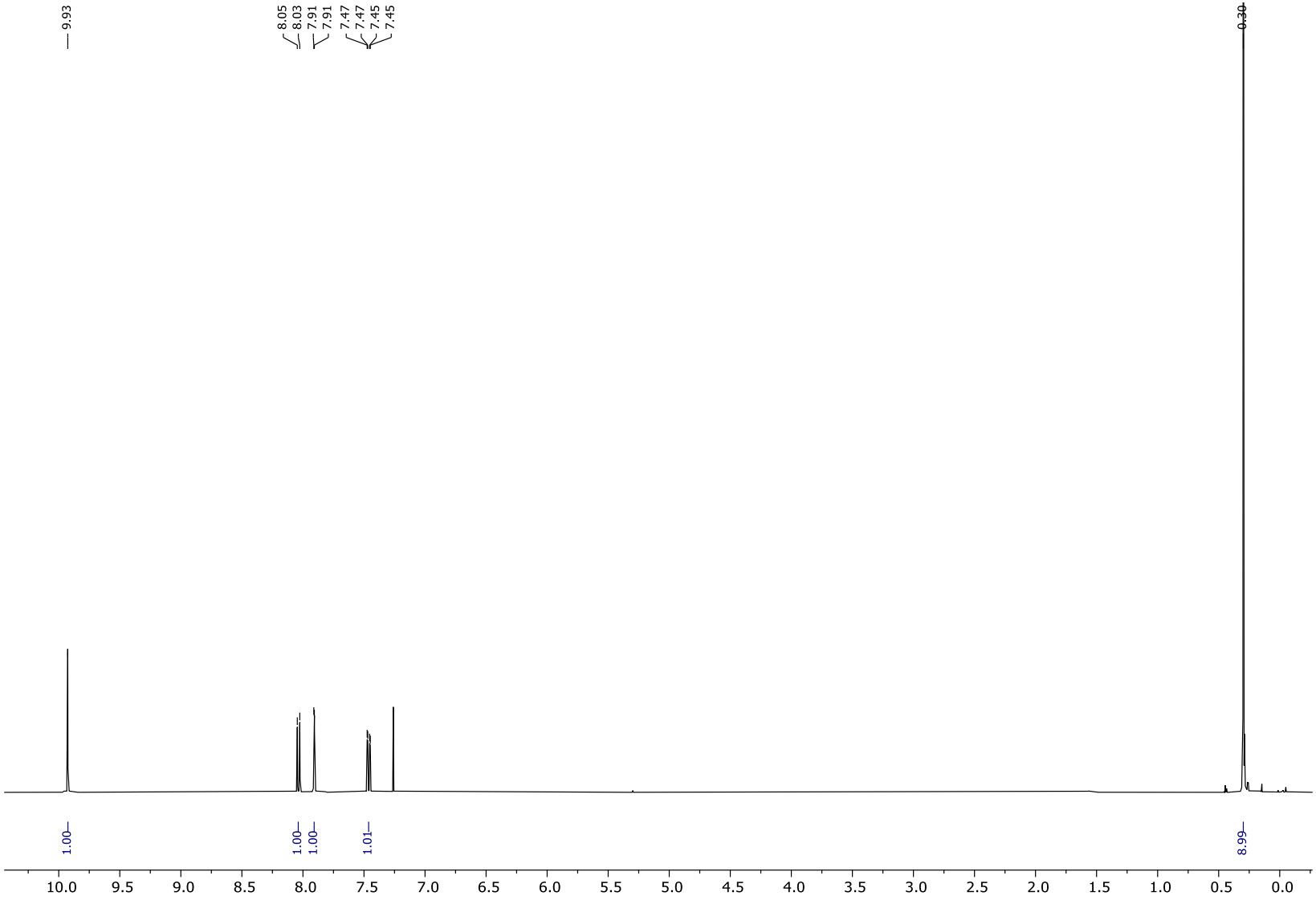

Figure S3. ^{1}H NMR spectrum (400 MHz, 298 K) of compound **iii** in $CDCl_3$.

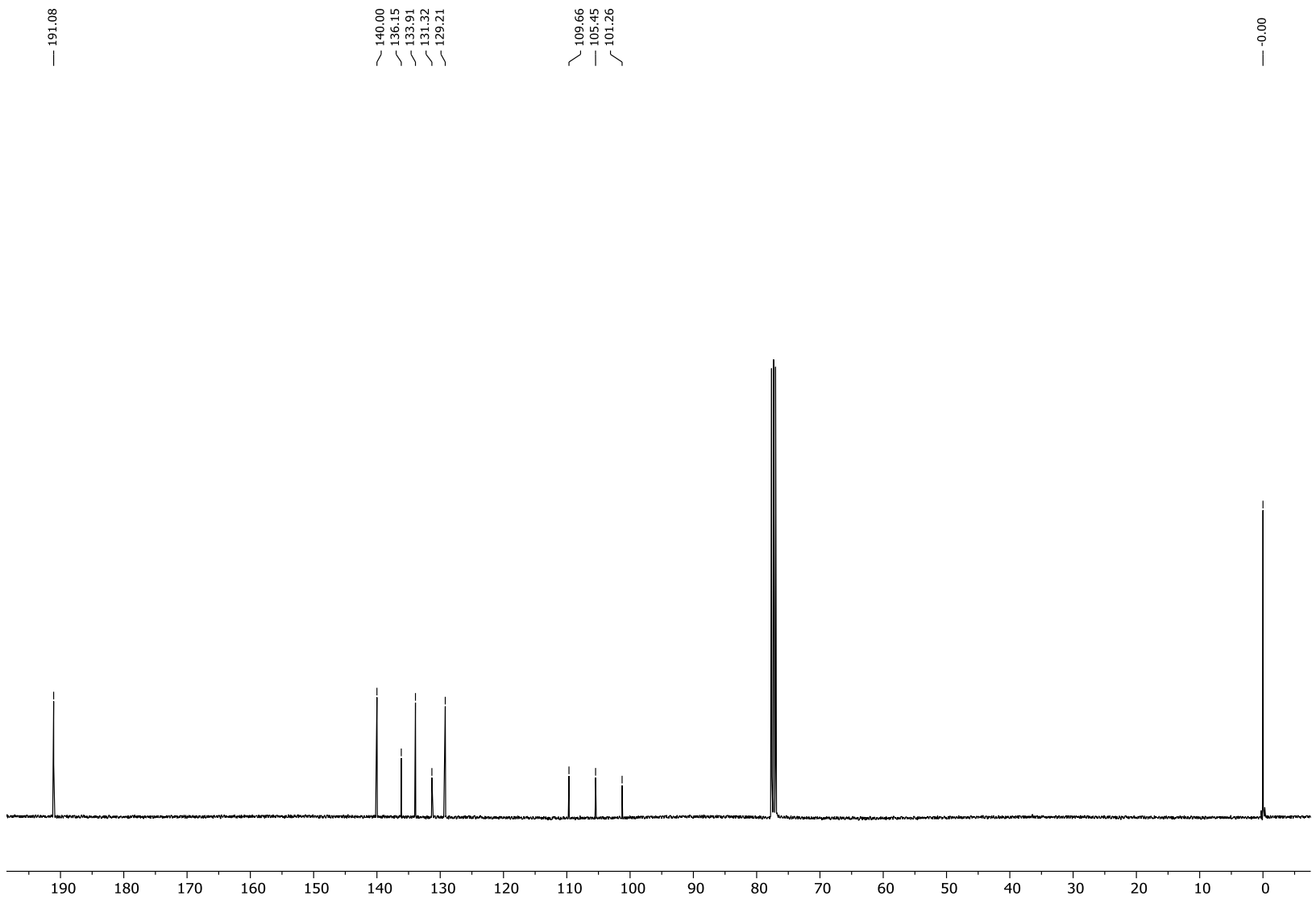

Figure S4. ^{13}C NMR spectrum (100 MHz, 298 K) of compound **iii** in $CDCl_3$.

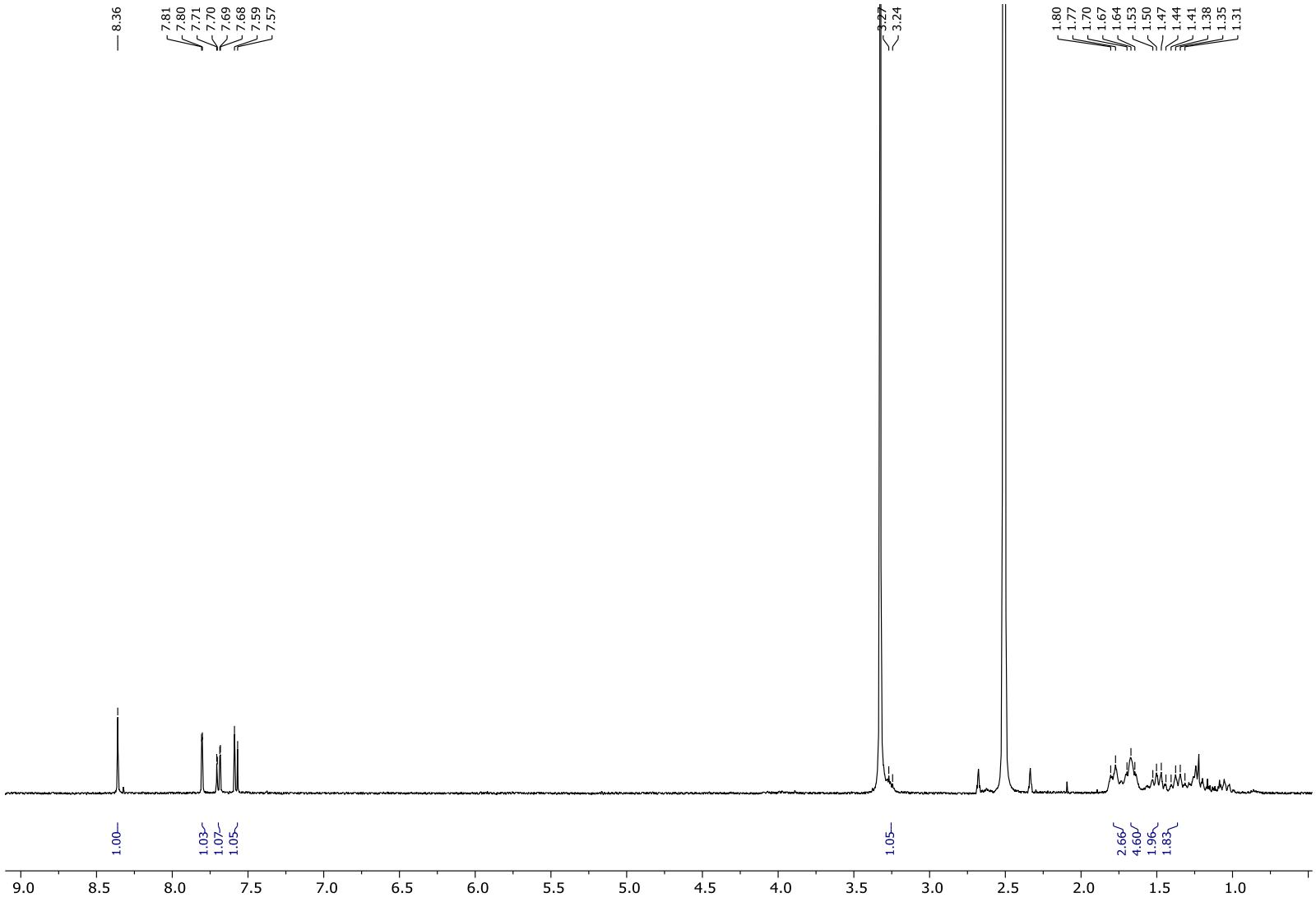

Figure S5. ^{1}H NMR spectrum (800 MHz, 298 K) of compound **4** in DMSO-d_6.

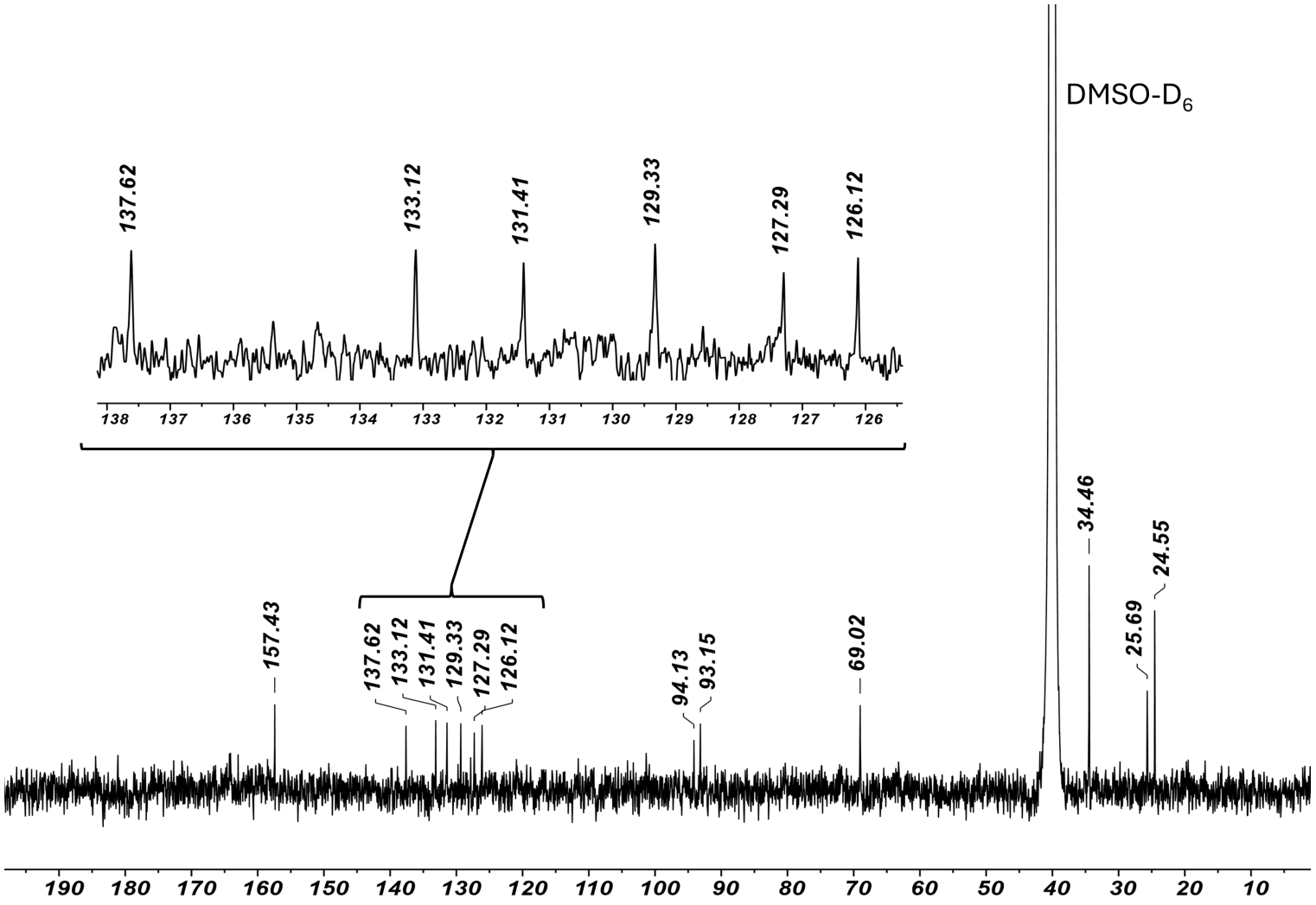

Figure S6. ^{13}C NMR spectrum (214 MHz, 298 K) of compound **4** in DMSO-d_6.

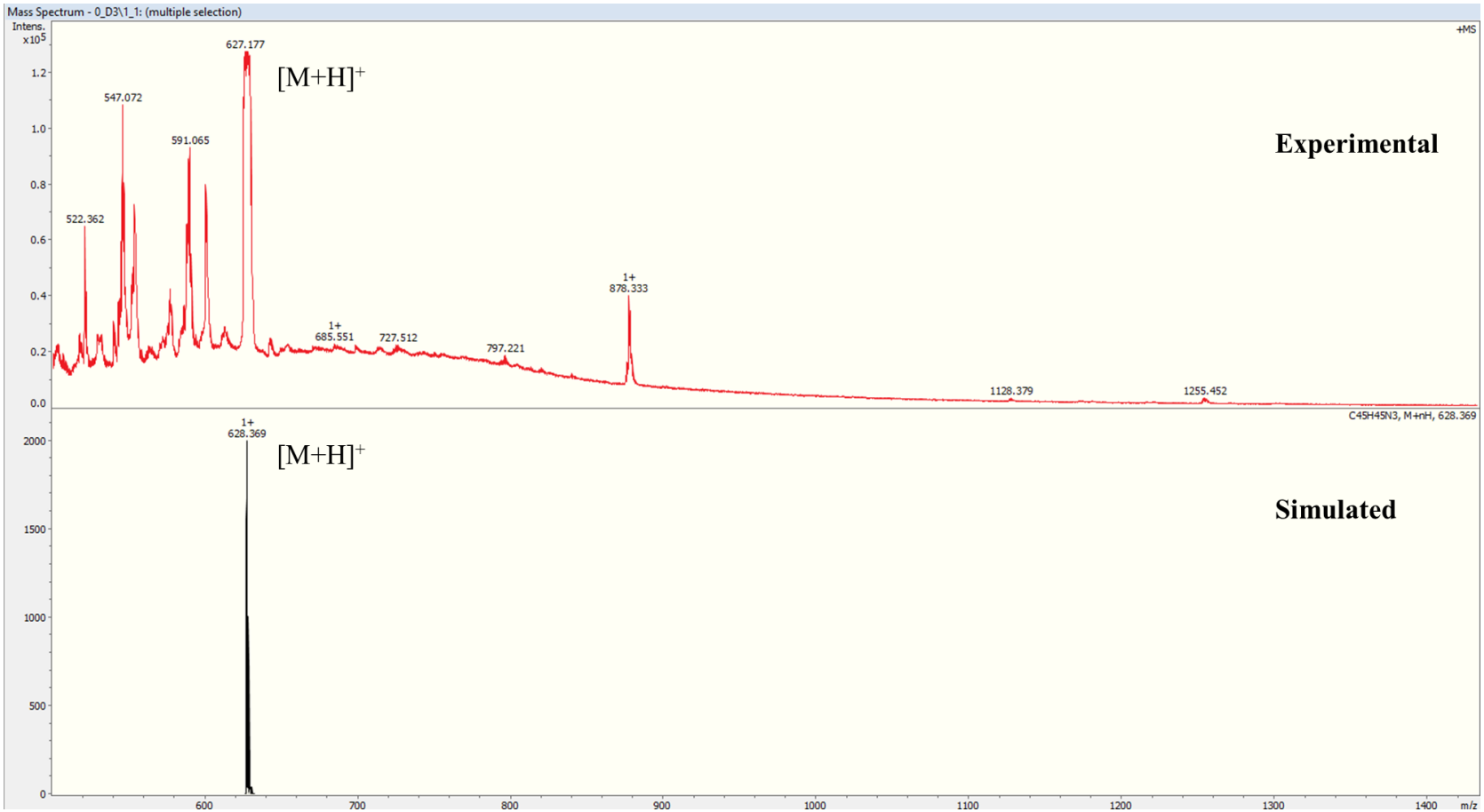
Mass Spectrum - 0_D3\1_1: (multiple selection)
Intens.
x10^5
+MS
627.177
[M+H]+
547.072
591.065
522.362
1+
878.333
1+
685.551
727.512
797.221
1128.379
1255.452
Experimental
C45H45N3, M+nH, 628.369
1+
628.369
[M+H]+
Simulated
m/z

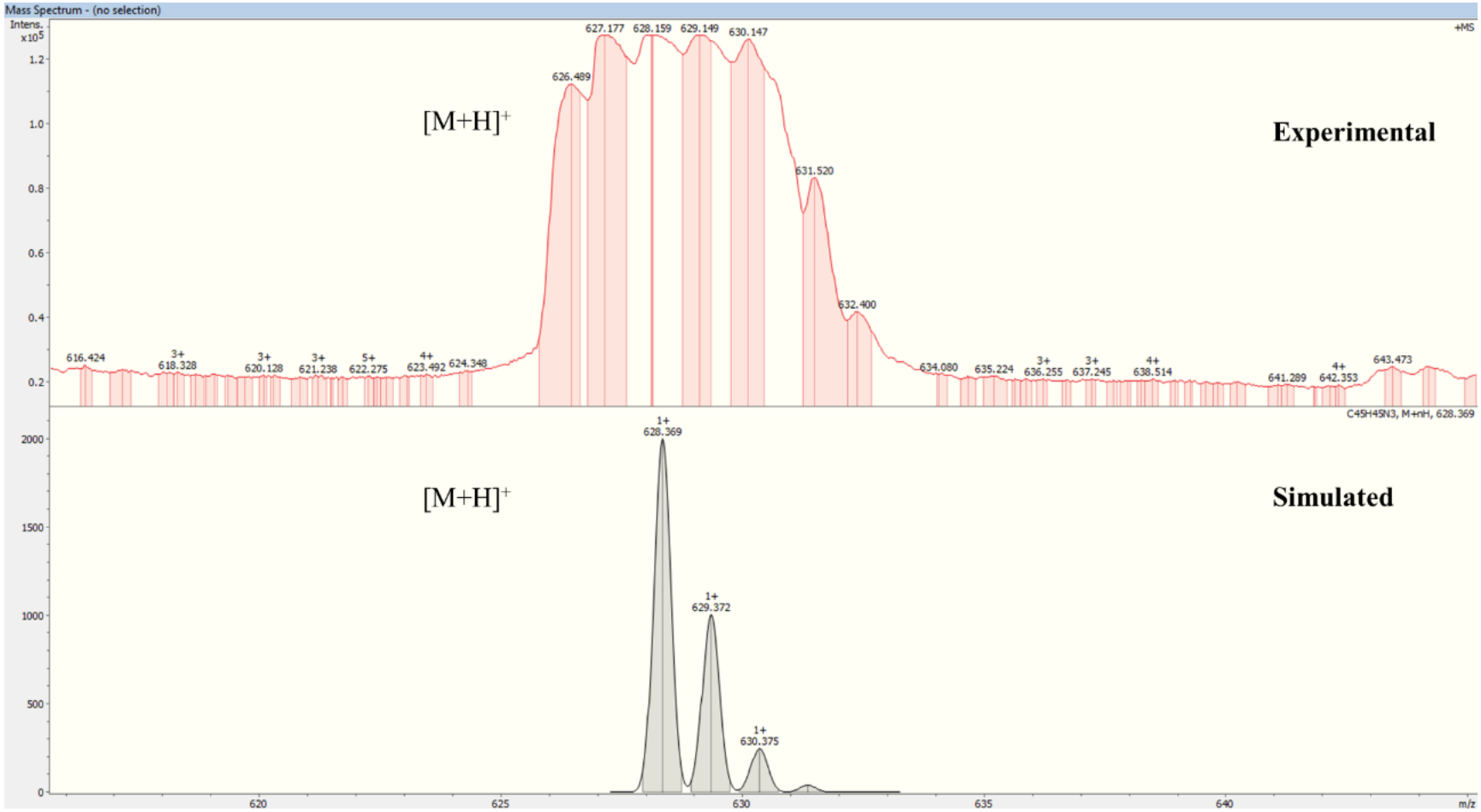

Figure S7. (Top) MALDI-MS of compound **4** (matrix: DCTB; positive reflector mode). (Bottom) The largest signal is zoomed in showing an ion with the mass 628.159 which is close to simulated [**4**+H]$^+$ cation (bottom) at 628.369.

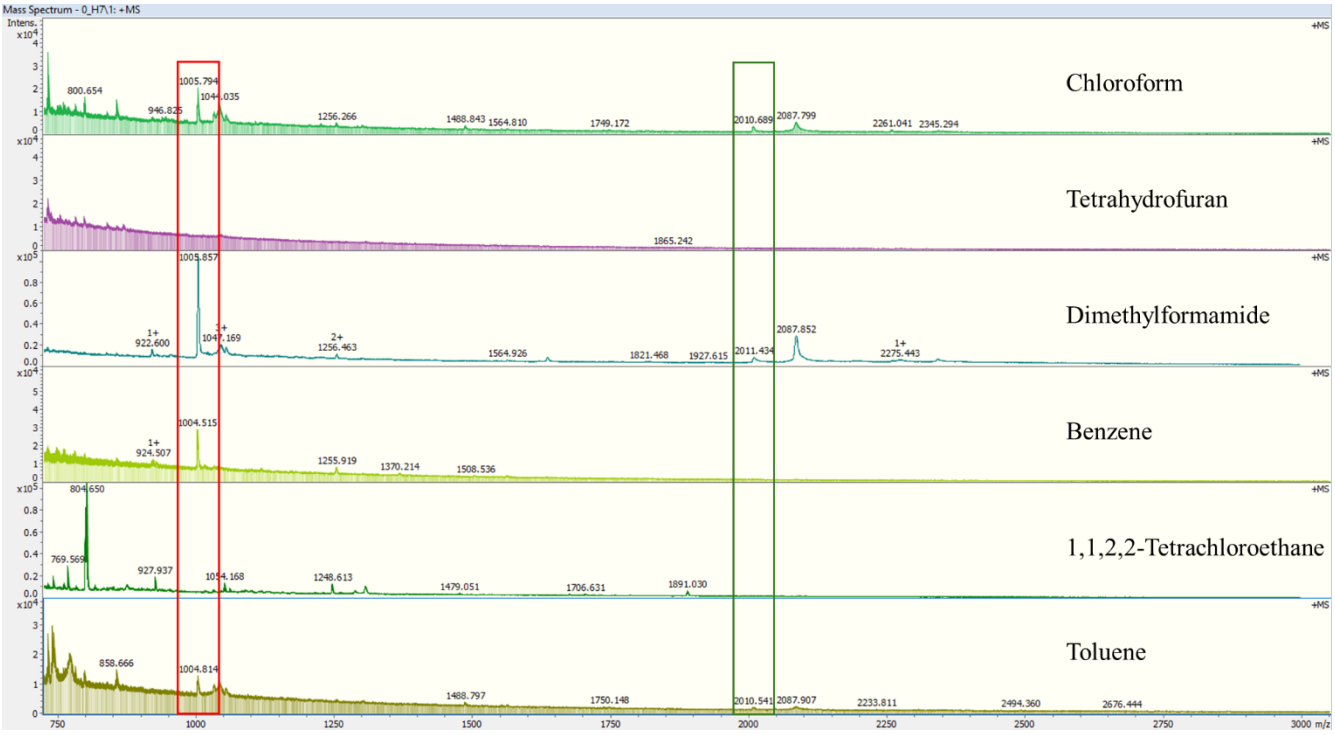

Figure S8. Dynamic imine condensation of DBA **2** and *R*-CDA was monitored in six solvents using MALDI spectrometer (9-nitroanthracene as matrix; positive reflectron mode). Red and green boxes show two regions with ions whose mass corresponds to [2+3] cage **1** and/or [4+6] cage **3** (see Figure 1B in main text). The lower resolution of data from low mass MALDI measurement prevented isotope distribution analysis. **General procedure**: DBA **2** (0.53 µmol) was combined with *R*-CDA (1.13 µmol) in 1 mL of the probed solvent. Trifluoroacetic acid (0.11 µmol) was added, and the reaction was stirred at 25 °C for 24 h. Next, 1 µL of a sample from the reaction was mixed with 1 µL of saturated matrix solution (9-nitroanthracene) in acetonitrile and spotted on a MALDI plate. Measurements were done in the linear reflectron mode. **Discussion**: The results of MALDI measurements show that imine condensations in chloroform, dimethylformamide, benzene, and toluene have a desired outcome. Dimethylformamide was not chosen for ^{1}H NMR studies due to limited solubility of DBA **2**. We disregarded chloroform since this solvent contains small amounts of acid giving inconsistent results when the reaction was monitored with ^{1}H NMR spectroscopy (not shown here). Finally, benzene and toluene remained as solvents of choice to study the condensation.

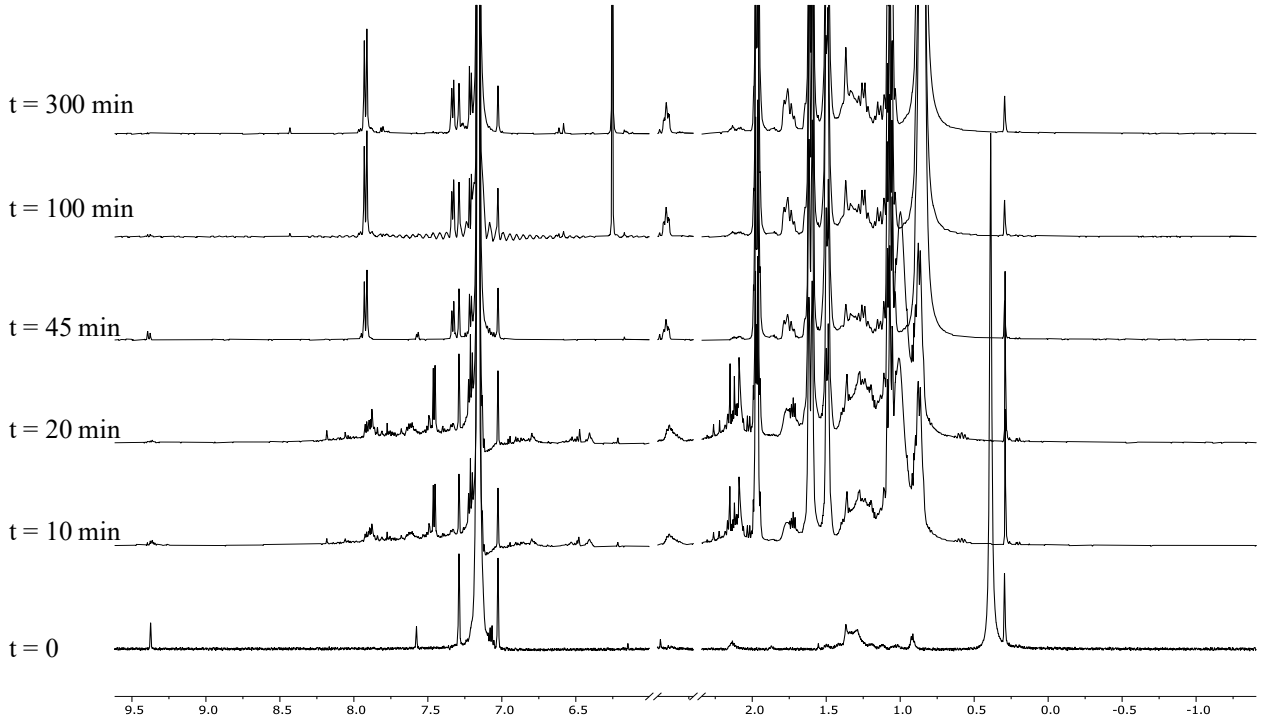

Figure S9. ^{1}H NMR spectra (600 MHz, C_6D_6) of DBA **2** (1.30 μmol), *R*-CDA (1.95 μmol), and 13 μL of trifluoroacetic acid (0.2eq) in 600 μL of C_6D_6 were recorded over 300 min.

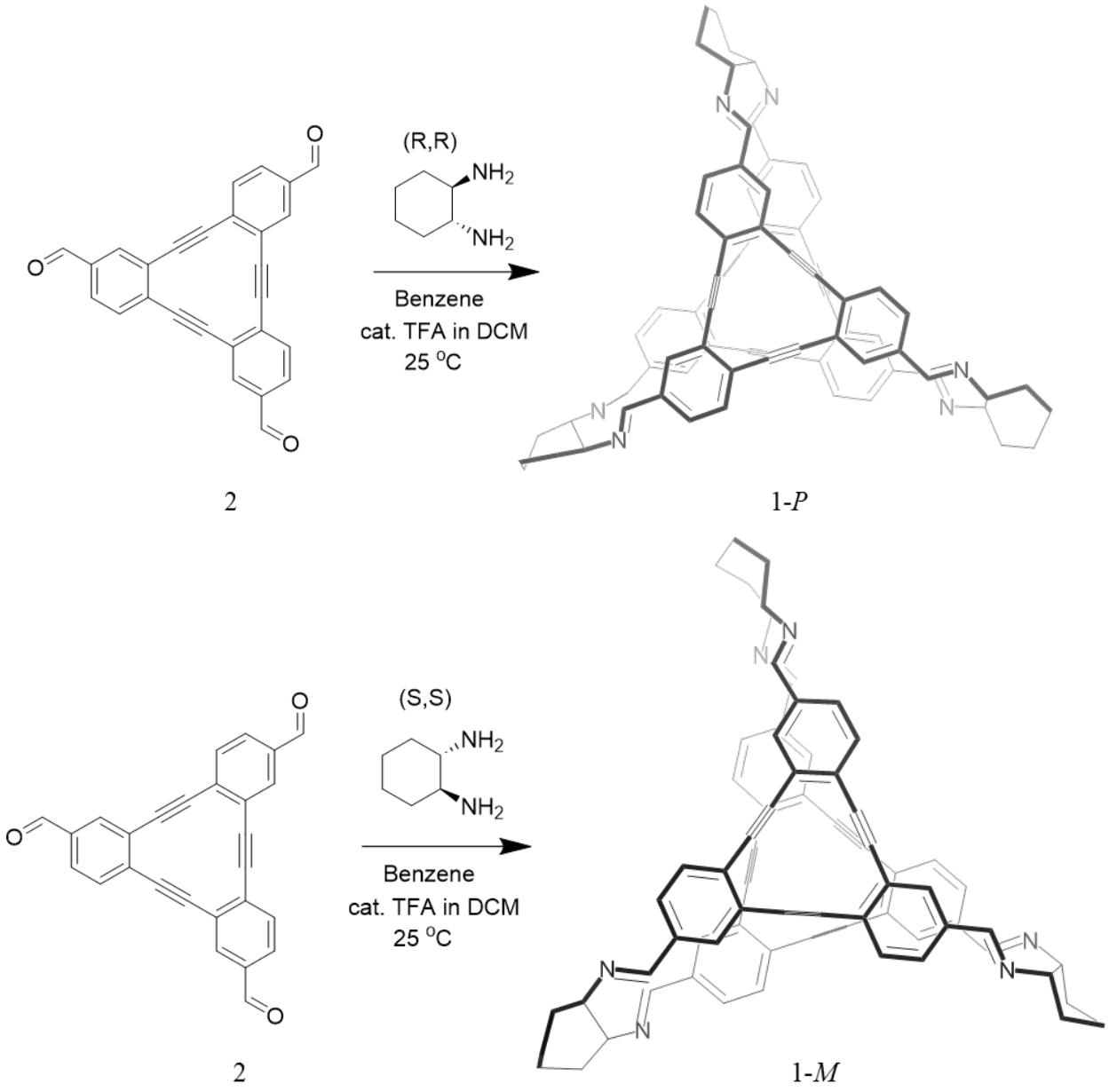

Scheme S4. Synthesis of cages **1**-*P* and **1**-*M* by condensation of DBA **2** with *R*-CDA (top) and *S*-CDA (bottom). **Cage 1-*P* and Cage 1-*M*.** To DBA **2** (5 mg, 13.0 μmol) in a round bottom flask was added benzene (10 mL) and a stirring bar. In a separate vial, (1*R*,2*R*)-cyclohexane-1,2-diamine (2.23 mg, 19.5 μmol; *R*-CDA) or (1*S*,2*S*)-cyclohexane-1,2-diamine (2.23 mg, 19.5 μmol; *S*-CDA) was dissolved in 3 mL of benzene followed by its transfer to the solution of DBA **2**. Next, 13 μL

of 20 mM trifluoroacetic acid in dichloromethane was added and the reaction mixture was allowed to stir for 8 h. After, the solution was filtered through a cotton plug and concentrated in vacuo; note that the reaction will begin as a suspension and then turn transparent over this time. Anhydrous methanol (5 mL) was added, and the mixture sonicated for 60 s. The resulting suspension was centrifuged for 5 minutes at 6000 rpm, the organic layer removed, and the solid left to dry giving cage **1**-*P* (12 mg, 91 %) or **1**-*M* (11.5 mg, 88%) as a bright yellow solid. ^{1}H NMR (600 MHz, C_6D_6) δ (ppm): 7.64 (dd, 8 Hz, 1H), 7.5 (s, 1H), 7.29 (d, 8 Hz, 1H), 6.66 (d, 2 Hz, 1H), 3.16-3.14 (m, 1H), 2.08-2.06 (m, 1H), 1.88-1.86 (m, 2H), 1.52-1.49 (m, 1H). ^{13}C NMR (214 MHz, C_6D_6) δ (ppm): 163.62, 136.40, 134.47, 132.12, 129.24, 124.90, 94.55, 94.13, 75.78, 24.87, 23.14. HRMS (ESI): *m*/*z* calculated for $C_{72}H_{54}N_6$: 1003.4488 $[M+H]^+$, found: 1003.4476 (Figure S12).

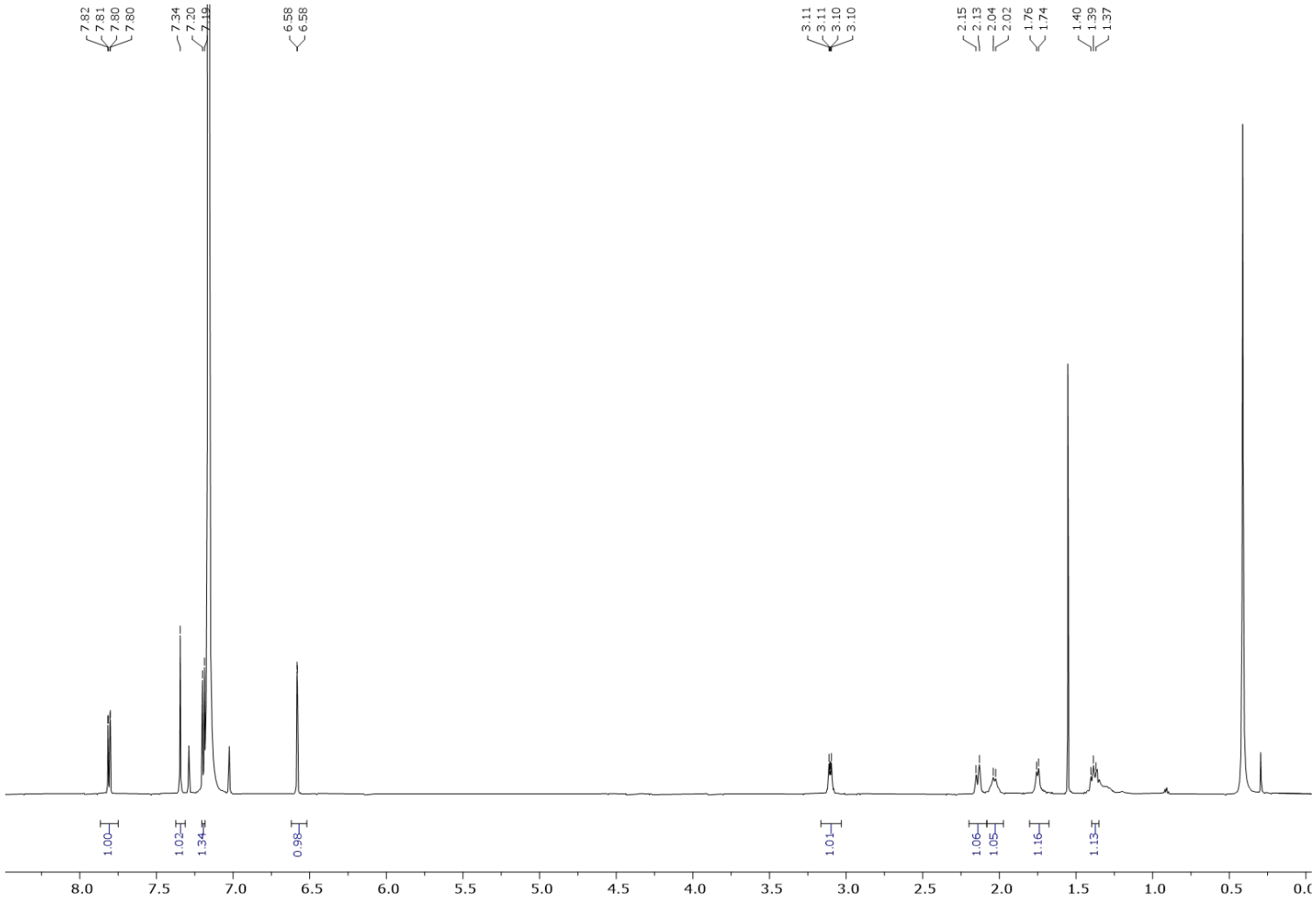

Figure S10. ^{1}H NMR spectrum (600 MHz, 298 K) of cage **1** from the imine condensation of DBA **2** and *R*-CDA in C_6D_6. Later in the text, product **1** is labeled as **1-*P***. Note that ^{1}H NMR spectrum of the product from the condensation of DBA **2** and *S*-CDA (i.e., **1**-*M*) is identical to **1**-*P* (Figure S16).

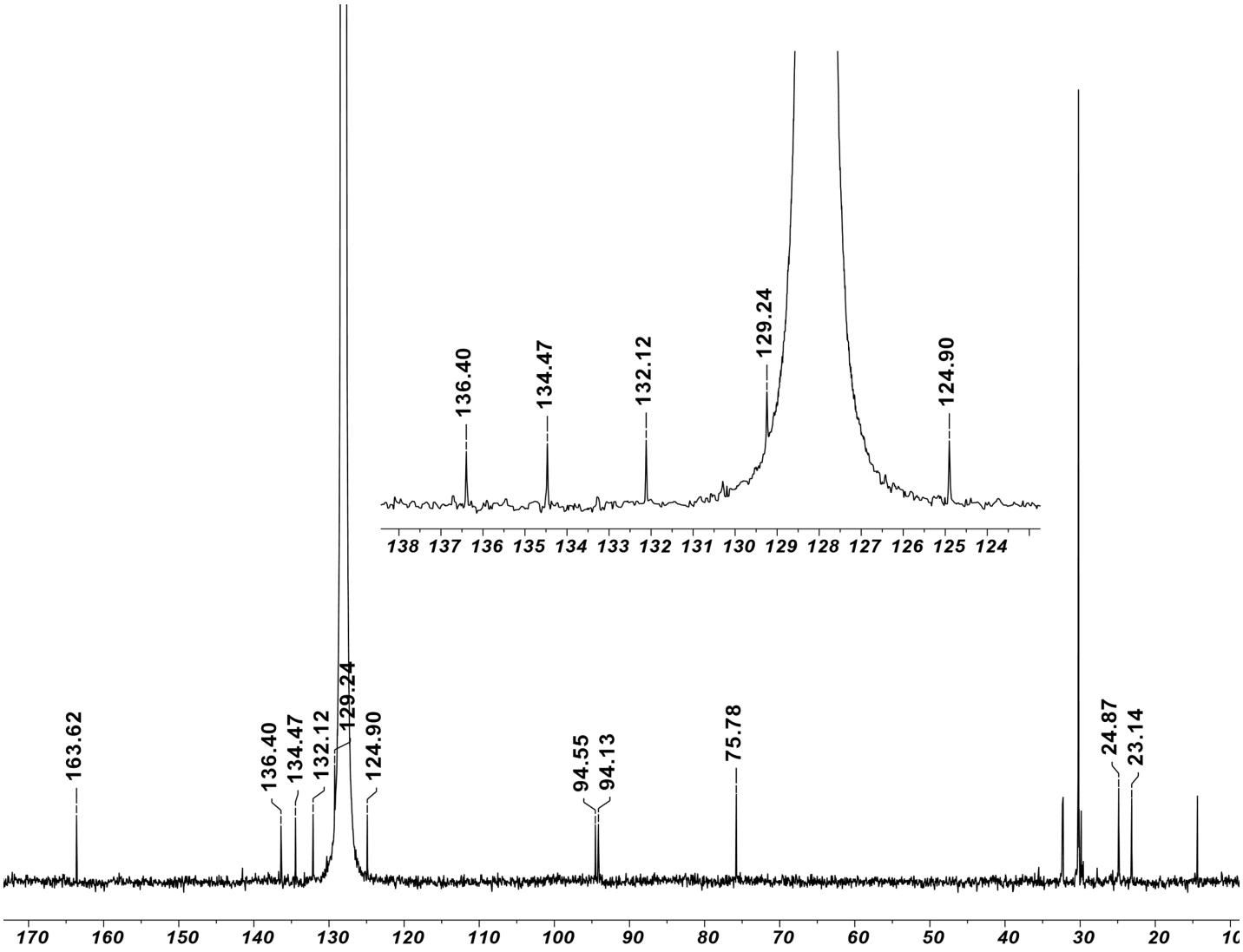

Figure S11. ^{13}C NMR spectrum (176 MHz, 298 K) of cage **1** from condensation of DBA **2** and *R*-CDA in C_6D_6. Later in text, product **1** is labeled as **1**-*P*. Note that ^{13}C NMR spectrum of the product from the condensation of DBA **2** and *S*-CDA (i.e., **1**-*M*) is identical to **1**-*P*.

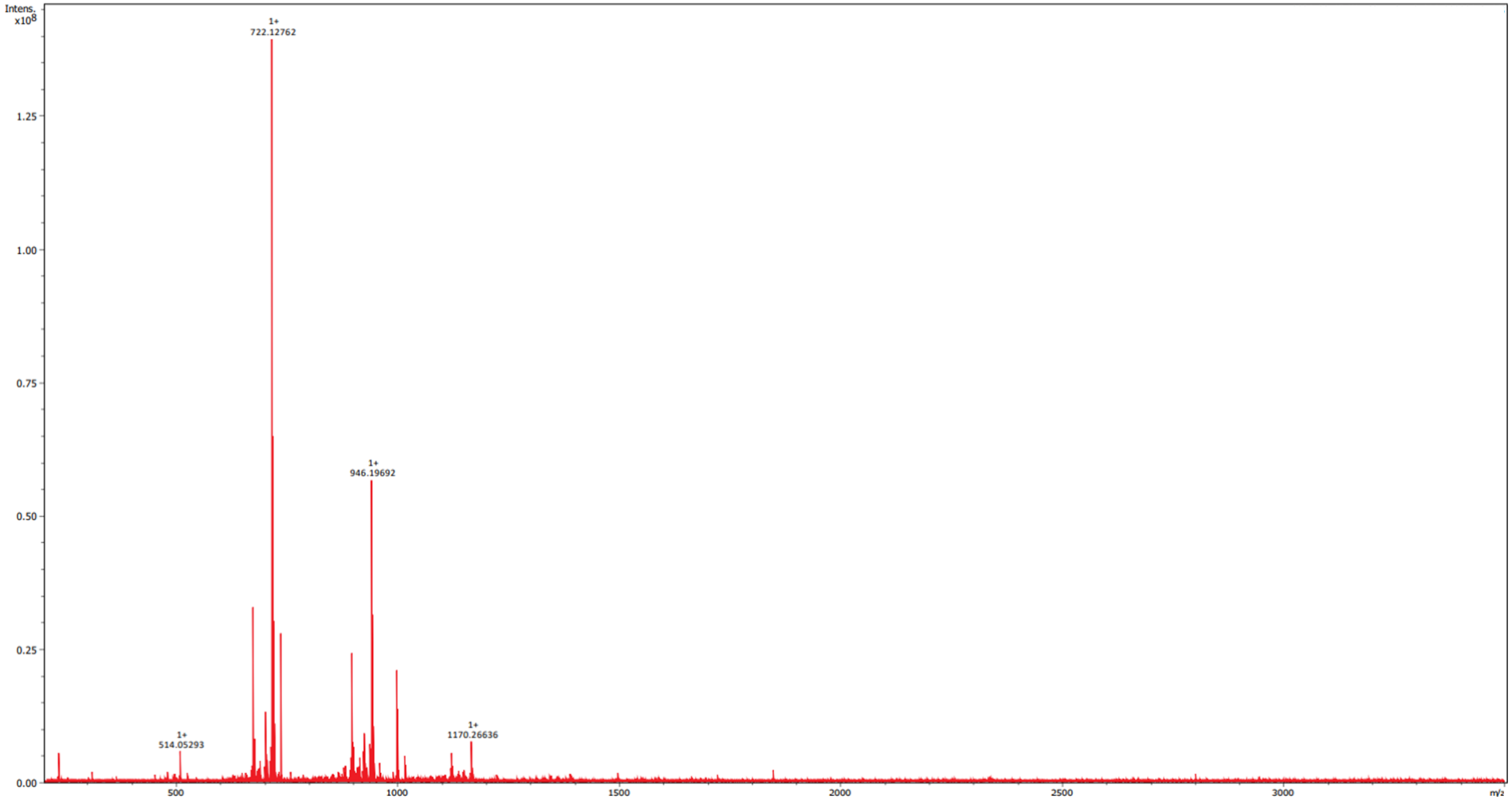
Intens.
x10^8
1.25
1.00
0.75
0.50
0.25
0.00
1+
722.12762
1+
946.19692
1+
514.05293
1+
1170.26636
500
1000
1500
2000
2500
3000
m/z

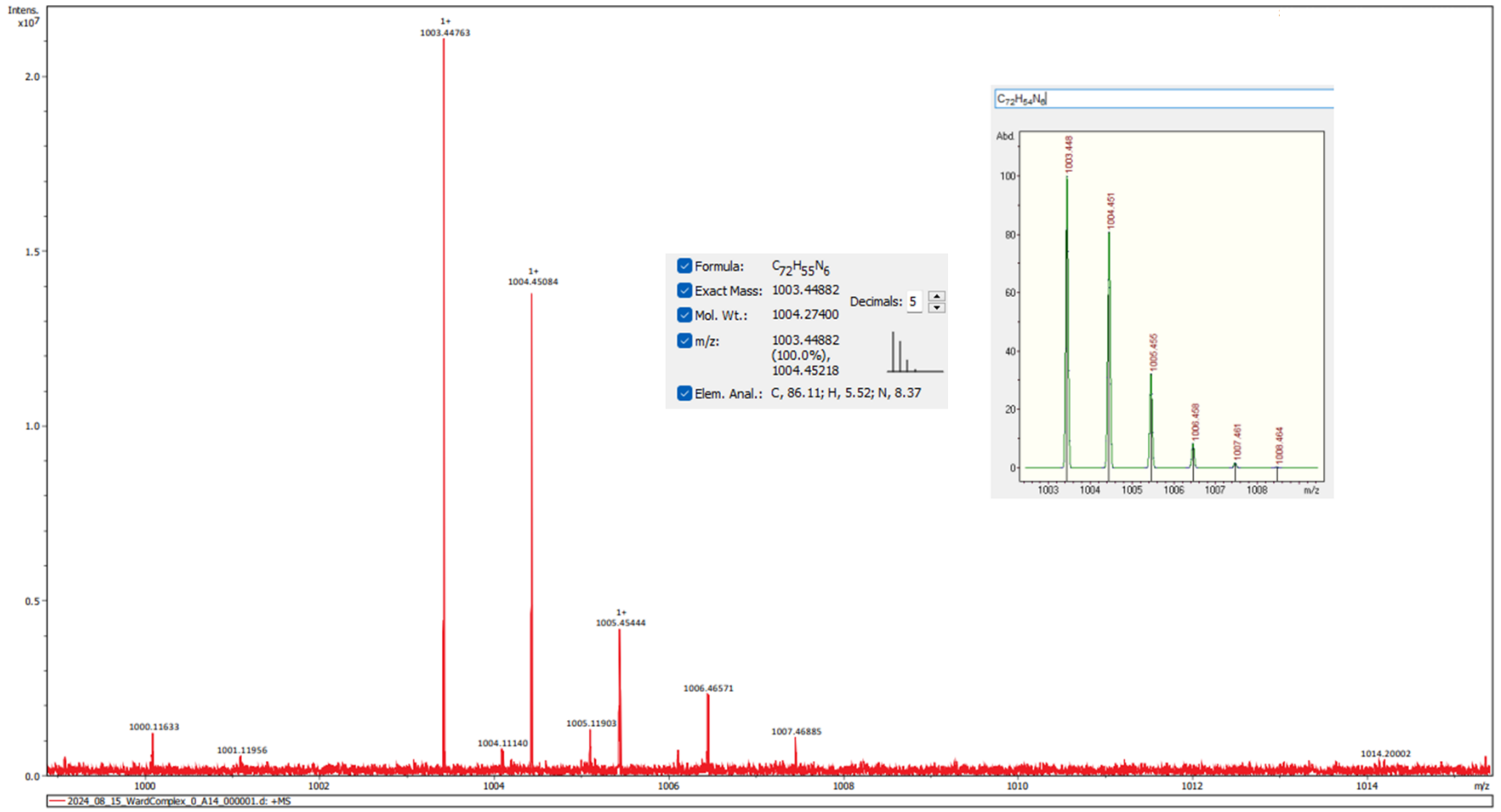

Figure S12: (Top) Experimental (red) mass spectrometry (ESI-MS) data for the observed ions from the product of condensation of DBA **2** and *R*-CDA. (Bottom) Experimental (red) and simulated (green) mass spectrometry (ESI-MS) data showing singly charged ion at 1003.4476 corresponding to [2+3] cage **1** (simulated mass,1003.4482) that we label **1-*P*** later in the text.

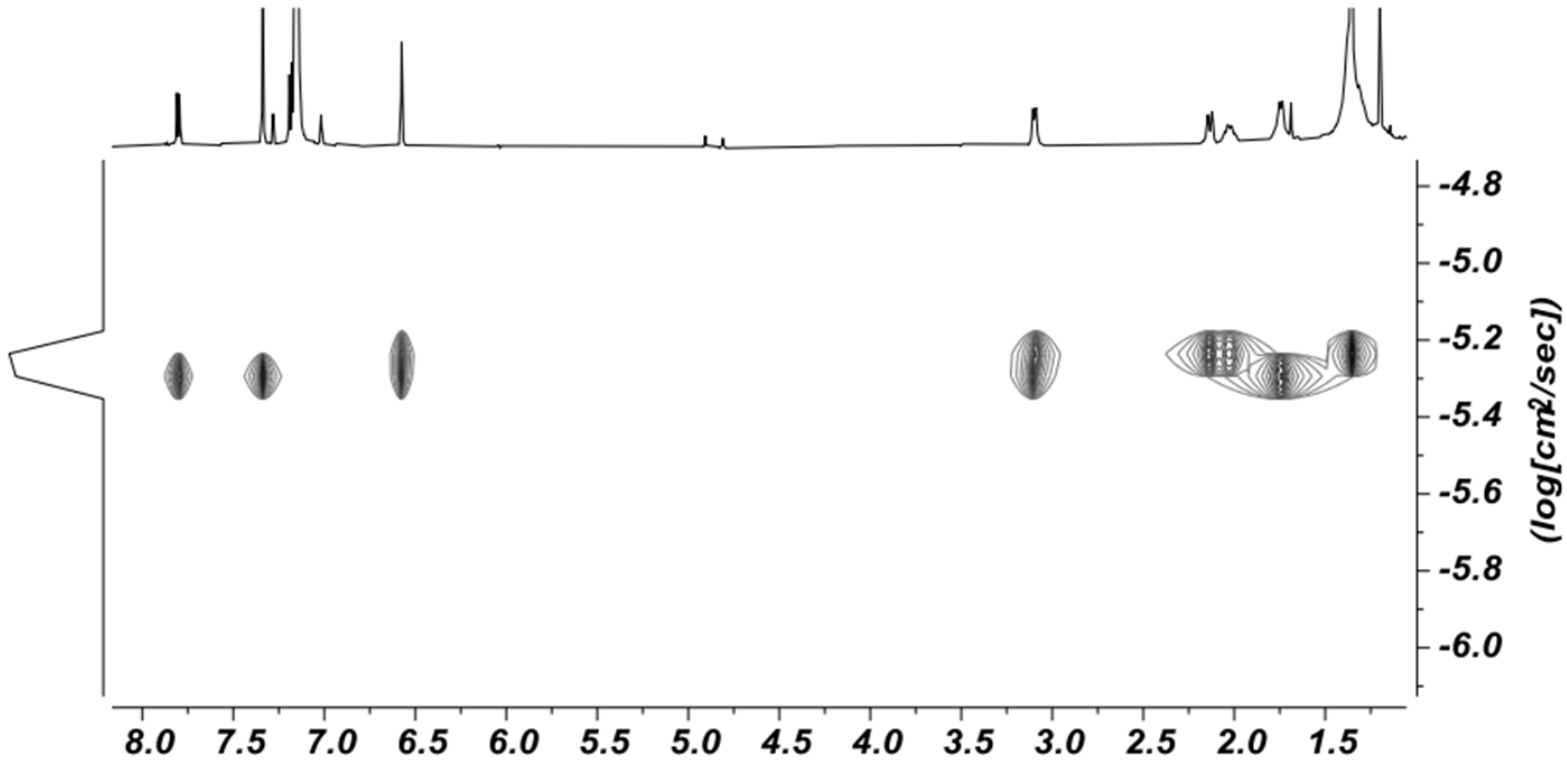
-4.8
-5.0
-5.2
-5.4
-5.6
-5.8
-6.0
(log[cm²/sec])
8.0
7.5
7.0
6.5
6.0
5.5
5.0
4.5
4.0
3.5
3.0
2.5
2.0
1.5

Index	Position (ppm)	Intensity	D (cm^2/s)	D_error
1	7.81	46.944	5.24756E-06	1.22504E-07
2	7.807	42.61	5.42442E-06	8.68959E-08
3	7.796	44.884	5.23503E-06	6.97358E-08
4	7.794	44.237	5.45001E-06	8.88278E-08
5	7.338	143.621	5.36515E-06	1.89256E-08
6	6.575	88.16	5.03981E-06	1.02429E-07
7	6.573	84.753	5.56738E-06	7.43587E-08
8	3.105	33.749	5.38402E-06	8.55141E-08
9	3.088	34.474	5.46417E-06	6.29295E-08
10	2.145	28.216	5.54469E-06	1.0283E-07
11	2.122	30.746	5.0812E-06	8.45034E-08
12	2.038	19.331	5.19005E-06	1.21283E-07
13	2.015	18.767	5.5525E-06	1.32434E-07
14	1.752	39.23	4.94383E-06	5.73469E-08
15	1.735	39.915	5.10496E-06	5.43473E-08
16	1.354	247.842	6.21154E-06	3.99252E-08
			5.3629E-06	

Figure S13. (Top) ^{1}H NMR DOSY spectrum (600 MHz, 298 K) of cage **1** (also labeled as **1-*P***) in C_6D_6. The DOSY data were processed in MestReNova (i.e., Furrier transformation, phasing, and baseline correction). (Bottom) Changes in the intensity of ^{1}H NMR resonances from **1** as a function of the magnetic field gradient strength *g* (G/cm) were fit using peak fit method in MestReNova v15.0.0-34764. For each proton nucleus, the corresponding diffusion coefficient *D* (m^2/s) were obtained (third column) from which the mean value (bottom)

was chosen for further analysis. Two Stokes Einstein equations were used to obtain hydrodynamic radii (see main text) with the viscosity of benzene η = 0.604 mPa·s at 298 K.

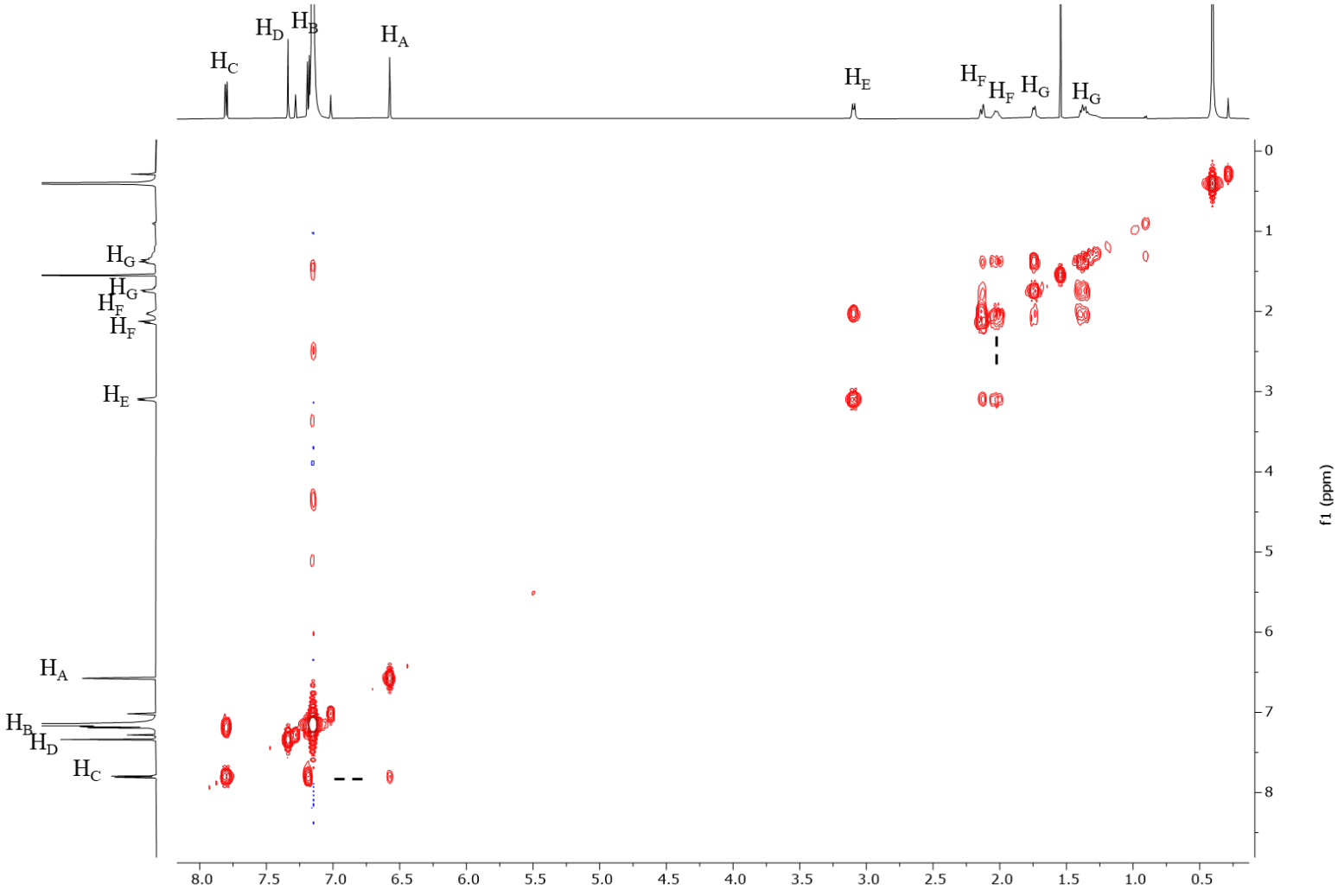

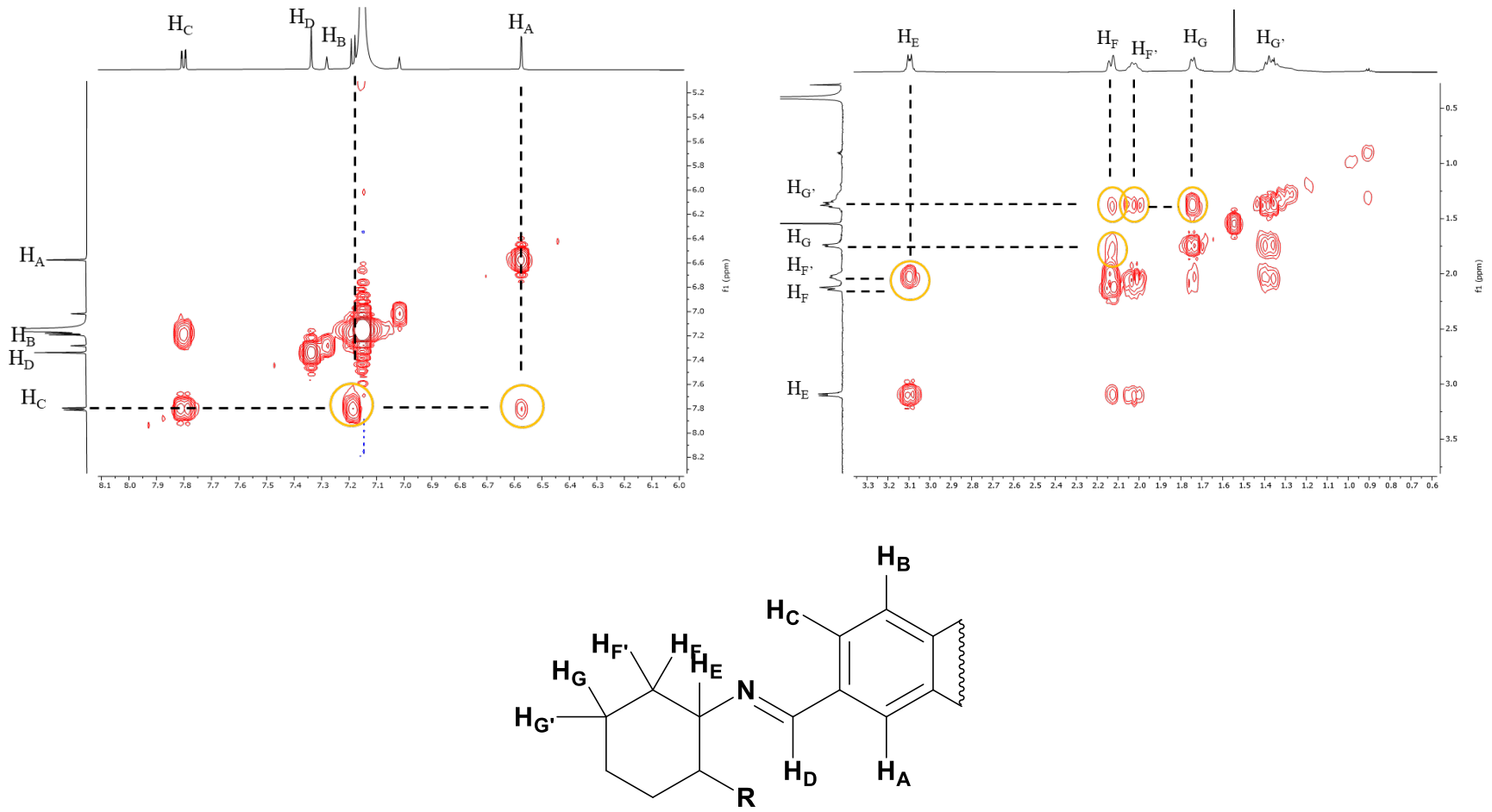

Figure S14. (Top) ^{1}H-^{1}H COSY spectrum (600 MHz, 298K) of cage **1** (i.e., **1**-*P*) in C_6D_6. (Bottom) Two segments from ^{1}H-^{1}H COSY spectrum of **1**, with labeled cross peak from scalar couplings. From the top segment, H_B couples with H_C while H_A shows a smaller set

of cross peaks with H_A (a long-range coupling). H_D remained isolated with no cross signals. From the second segment, H_E (the most deshielded proton of the cyclohexane ring) couples with diastereotopic $H_{F/F'}$. At last, $H_{F/F'}$ show cross peaks with $H_{G/G'}$.

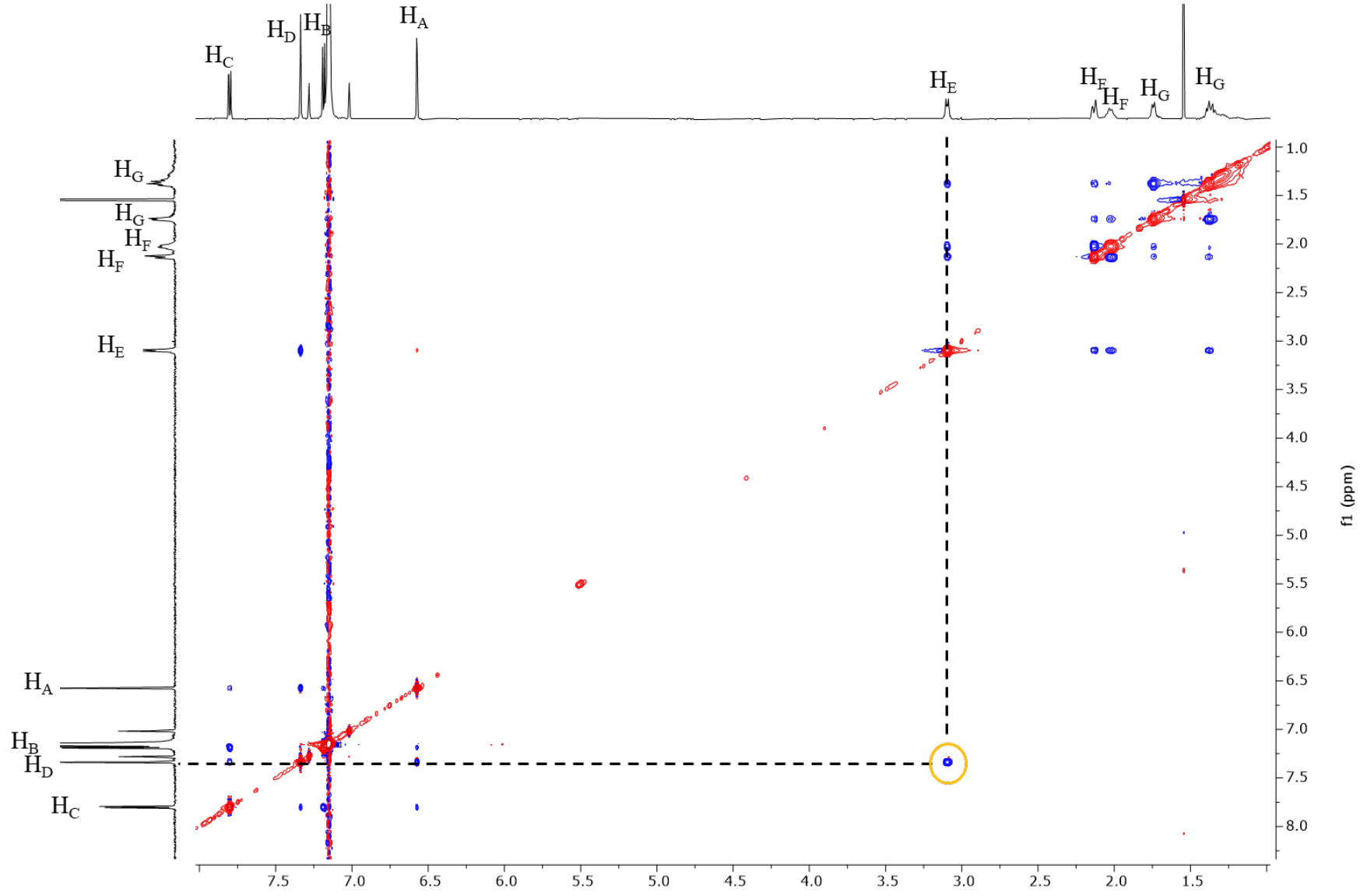

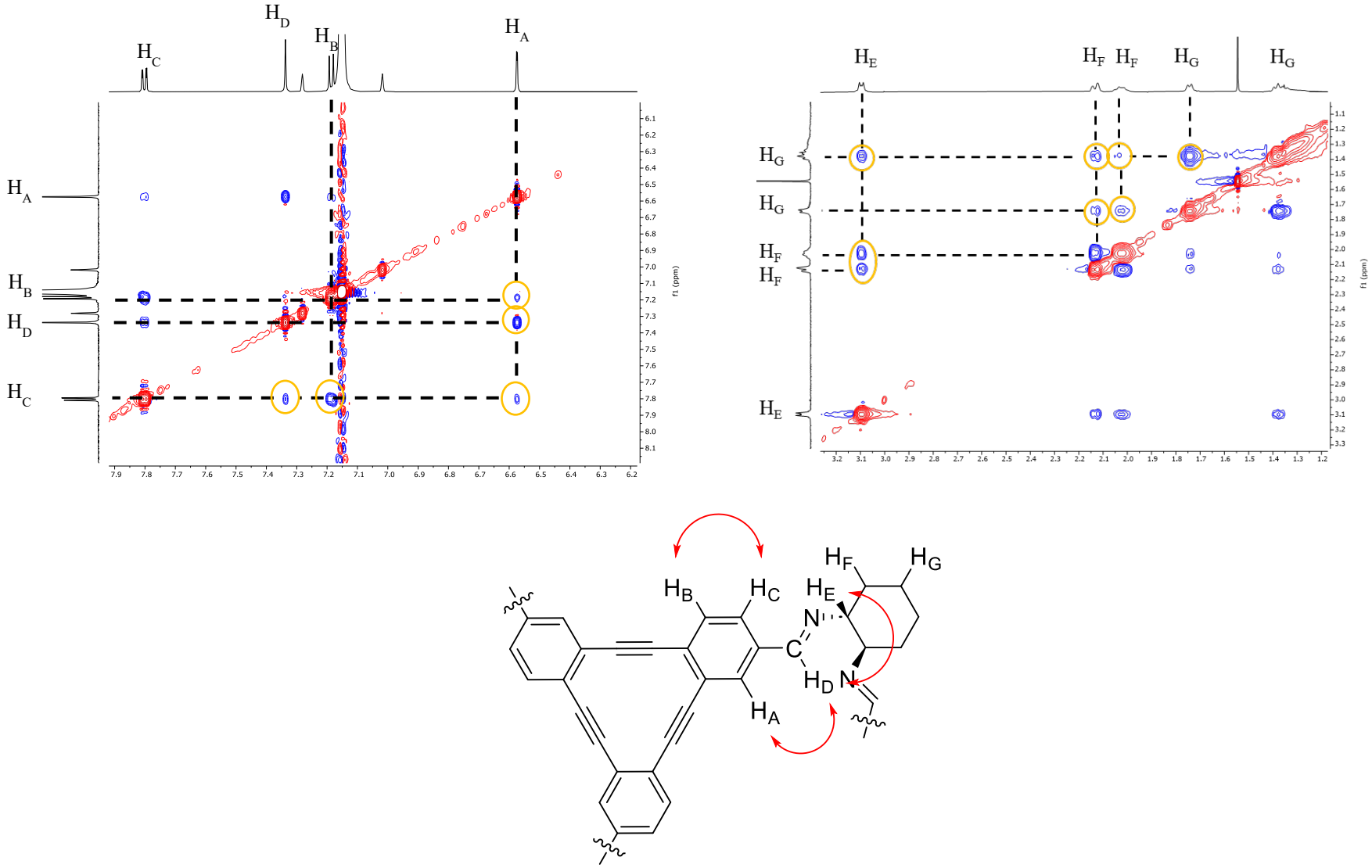

Figure S15. (Top) ^{1}H-^{1}H ROESY spectrum (600 MHz, 298 K) of cage **1** (i.e. **1**-*P*) in C_6D_6. Note the large cross peaks between H_E and H_D nuclei. (Bottom) Two segments of ROESY spectrum showing blue ROE cross peaks. From the left segment, a cross peak between H_D and H_A is stronger than H_D and H_C.

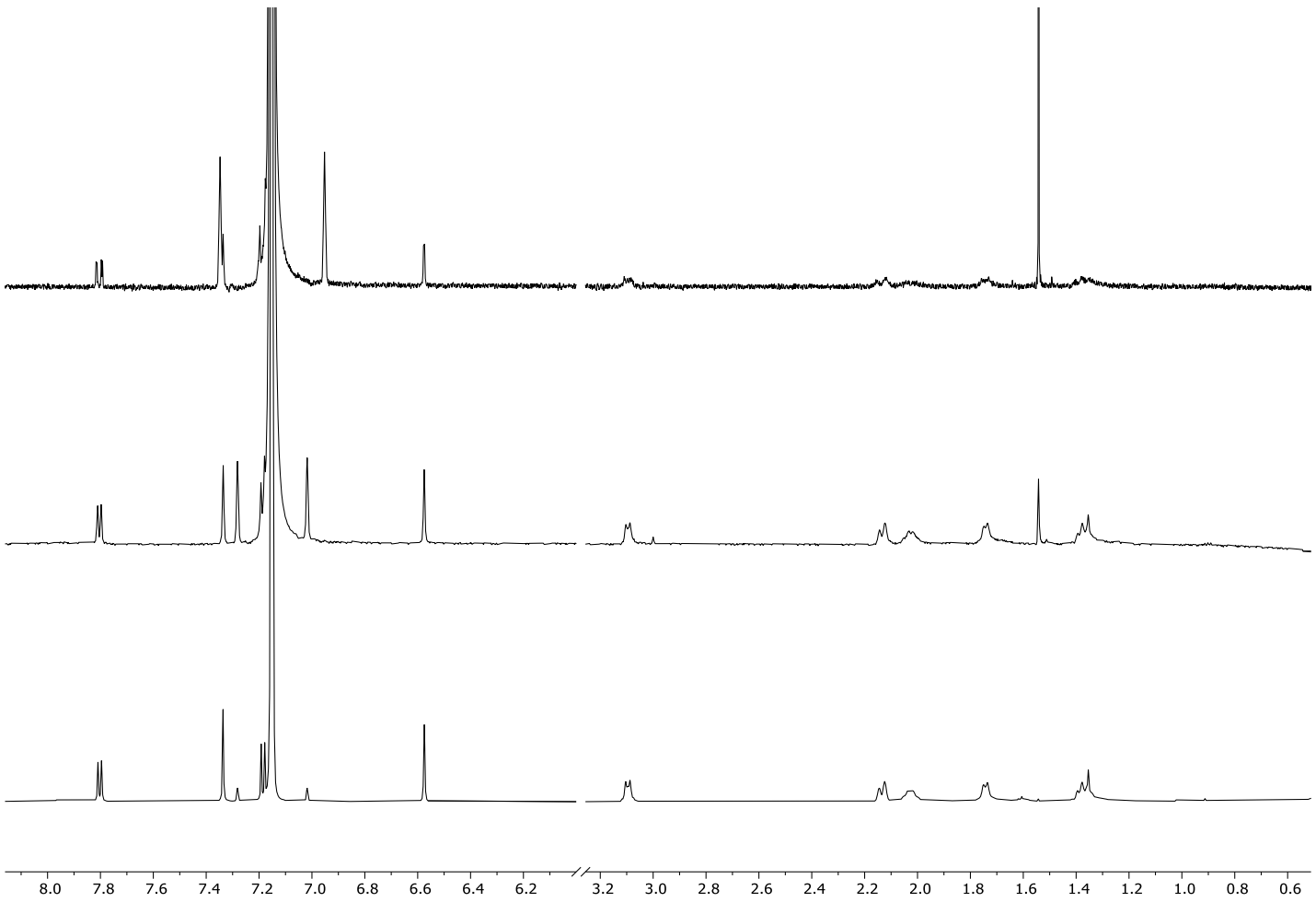

Figure S16. ^{1}H NMR spectra (600 MHz, 298K) of **1**-*P* (top, condensation of DBA **2** and *R*-CDA), **1**-*M* (middle; condensation of DBA **2** and *S*-CDA), and racemic **1**-***P/M*** (bottom, condensation of DBA **2** and racemic *R*/*S*-CDA) in C_6D_6.

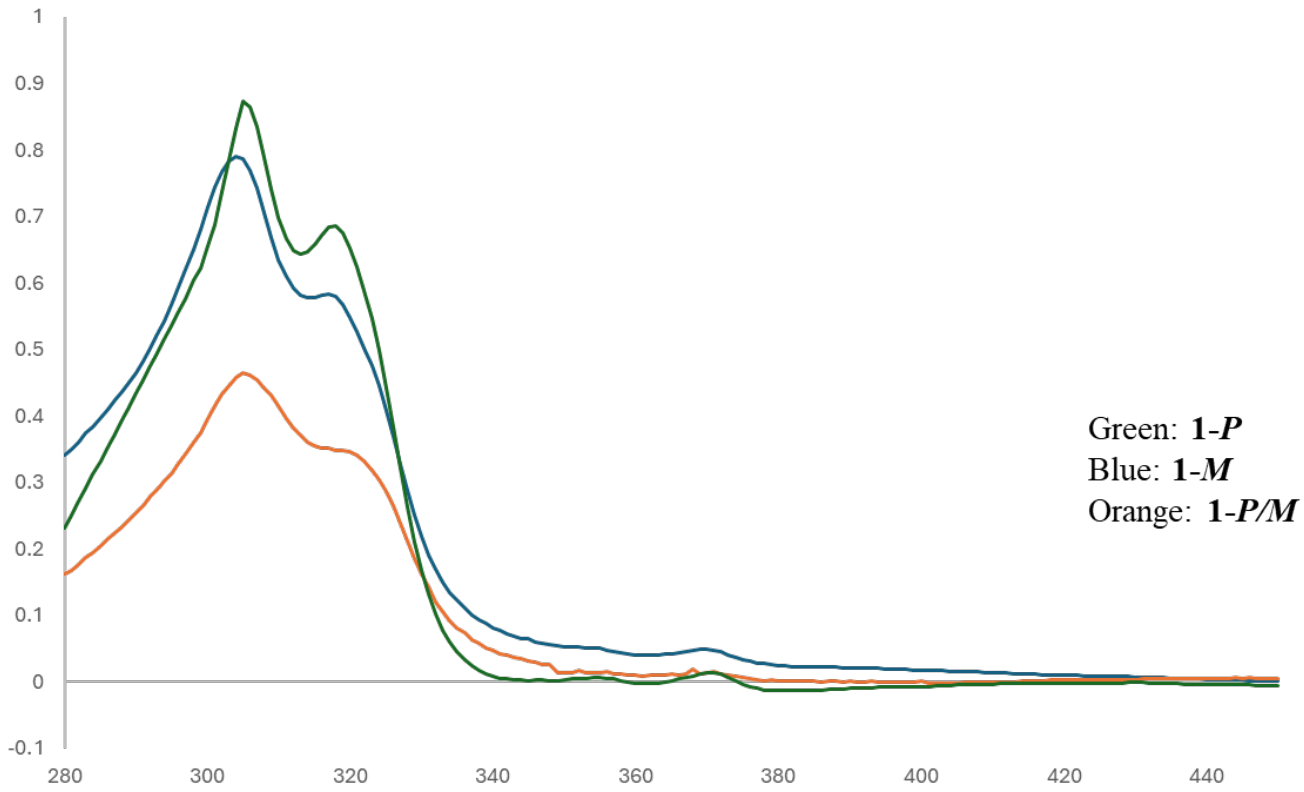

Figure S17. UV-Vis spectra of 53 μM solution of **1**-*P* (green), 40 μM solution of **1**-*M* (blue), and 20 μM solution of **1**-*P/M* (orange)in tetrahydrofuran.

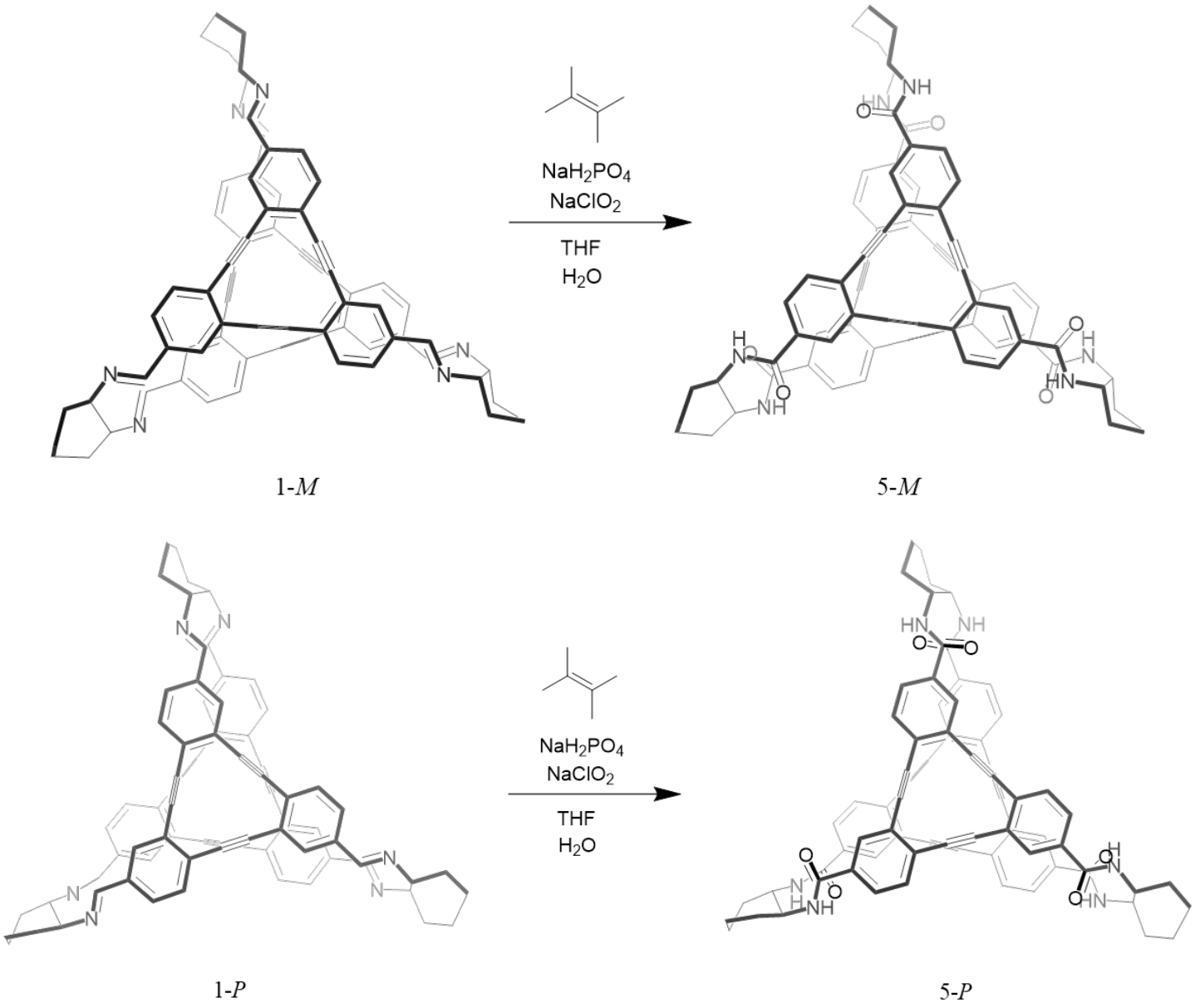

Scheme S5. A schematic representation of the Pinnick oxidation of **1**-*M* and **1**-*P* cages into robust amide cages **5**-*M* and **5**-*P*. **Cages 5-*M and* 5-*P***. To a vial containing THF (5 mL), $NaClO_2$ (27 mg, 0.29 mmol), and 2,3-dimethylbut-2-ene (59 µL, 0.49 mmol) was added 140 µL of 90 mM NaH_2PO_4 in water. After stirring for a few minutes, the solution turned pale yellow. Once the solution changed color, 5 mL of 1 mM solution of cage **1-*P*** (or **1-*M***) in anhydrous THF was added dropwise over 5 minutes. The solution was stirred vigorously overnight and diluted with 5 mL of EtOAc. The organic layer was washed with $NaHCO_3$ (2 x 5 mL), $Na_2S_2O_3$ (1 x 5 mL), H_2O (1 x 5 mL) and brine (1 x 5 mL), then dried over Na_2SO_4, filtered, and concentrated in vacuo. After, anhydrous methanol (5 mL) was added, and the mixture sonicated for 60 seconds. The resulting suspension was centrifuged for 5 minutes at 6000 rpm, the organic layer removed, and the solid

left to dry yielding amide cage **5**-*P* (3.8 mg, 69%) or **5**-*M* (4.1 mg, 74%) as a light-yellow solid. ^{1}H NMR spectra of **5**-*P* and **5**-*M* are identical (Figure S18). ^{1}H NMR (600 MHz, DMSO-d_6): δ (ppm) 7.96-7.95 (m, 1H), 7.73 (dd, J = 4 Hz, 1H), 7.39 (d, J = 4 Hz, 1H), 7.23 (d, J = 4 Hz, 1H), 4.01 (m, 1H), 1.84-1.83 (m, 2H), 1.66 (m, 1H), 1.36 (m, 1H). HRMS (ESI-MS): m/z calculated for $C_{72}H_{54}N_6O_6$: 1099.4177 $[M+H]^+$, found 1099.4178.

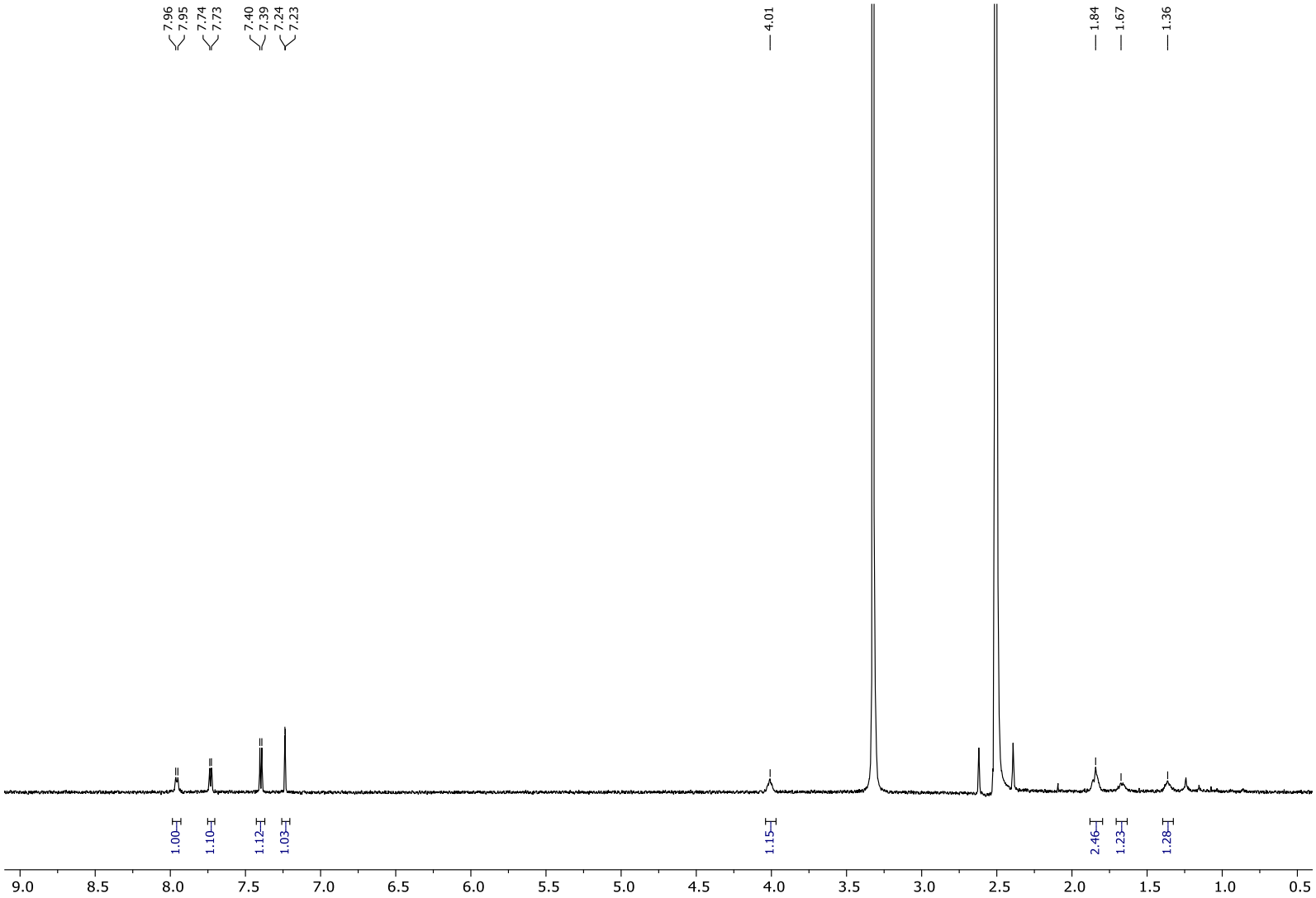
7.96
7.95
7.74
7.73
7.40
7.39
7.24
7.23
4.01
1.84
1.67
1.36
1.00
1.10
1.12
1.03
1.15
2.46
1.23
1.28
9.0
8.5
8.0
7.5
7.0
6.5
6.0
5.5
5.0
4.5
4.0
3.5
3.0
2.5
2.0
1.5
1.0
0.5

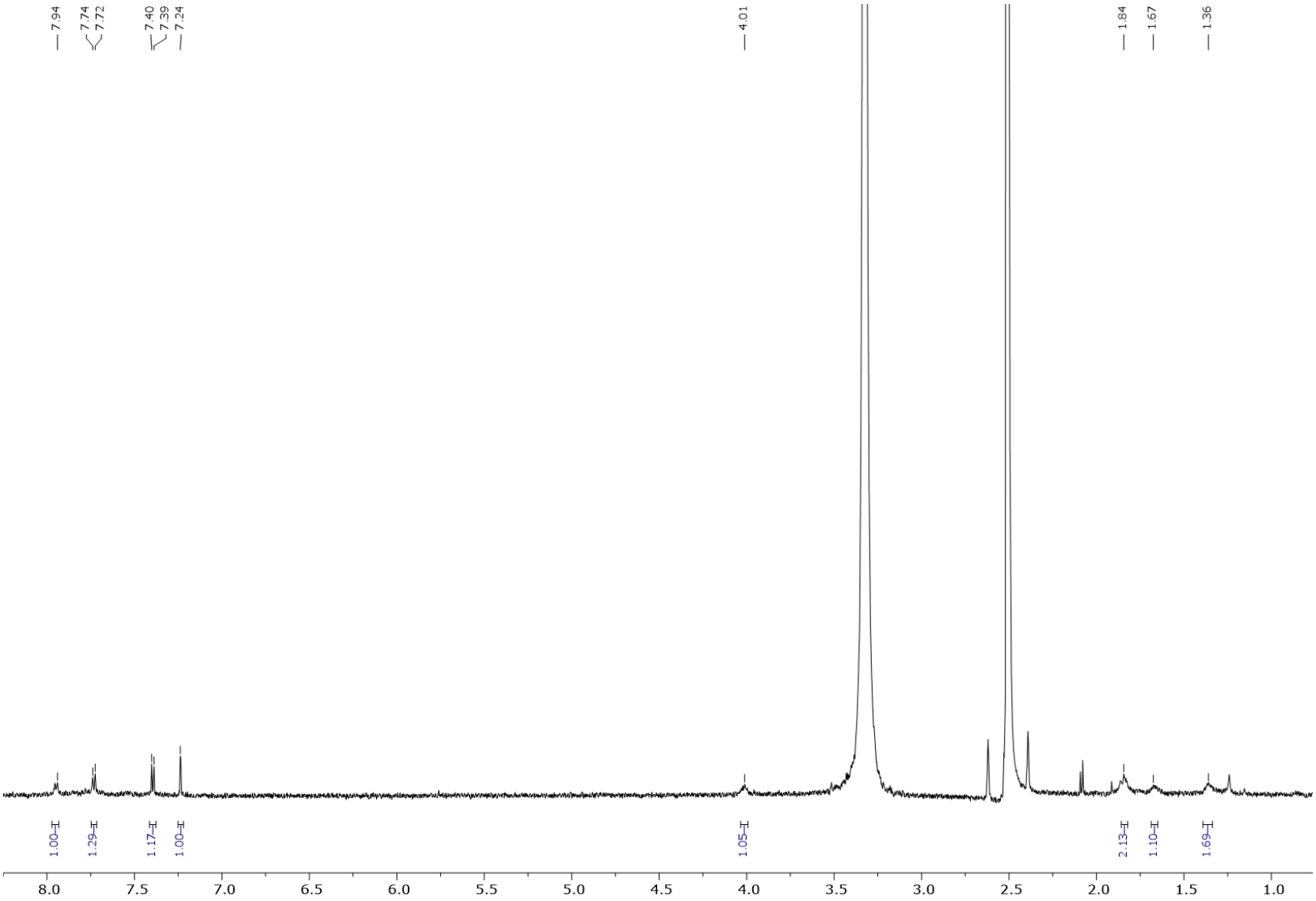

Figure S18. ^{1}H NMR spectra (600 MHz,298 K) of cages **5**-*P* (top) and **5**-*M* (bottom) in DMSO-d_6.

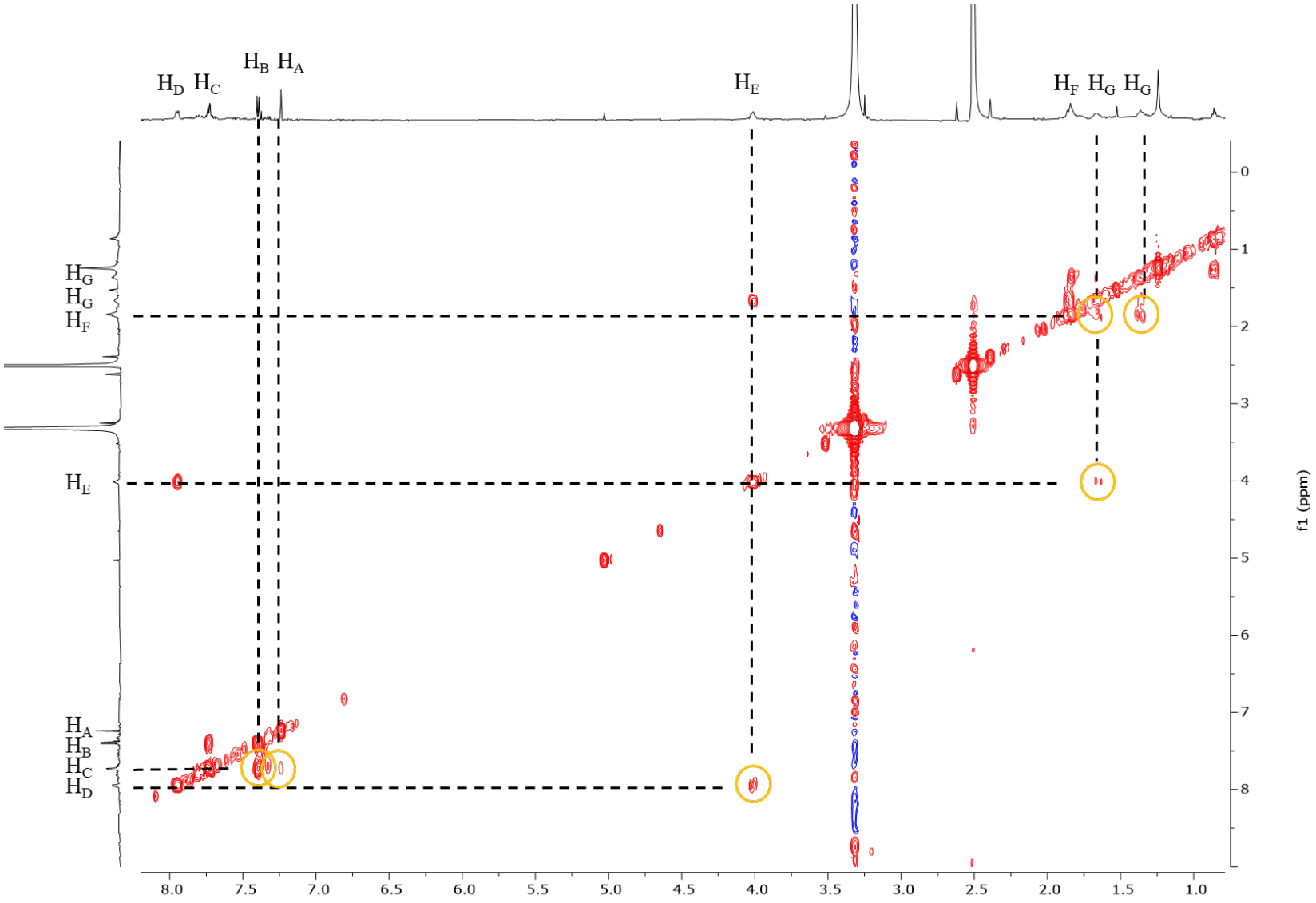

Figure S19. ^{1}H-^{1}H COSY (600 MHz, 298K) spectrum of cage **5-*P*** in DMSO-d_6.

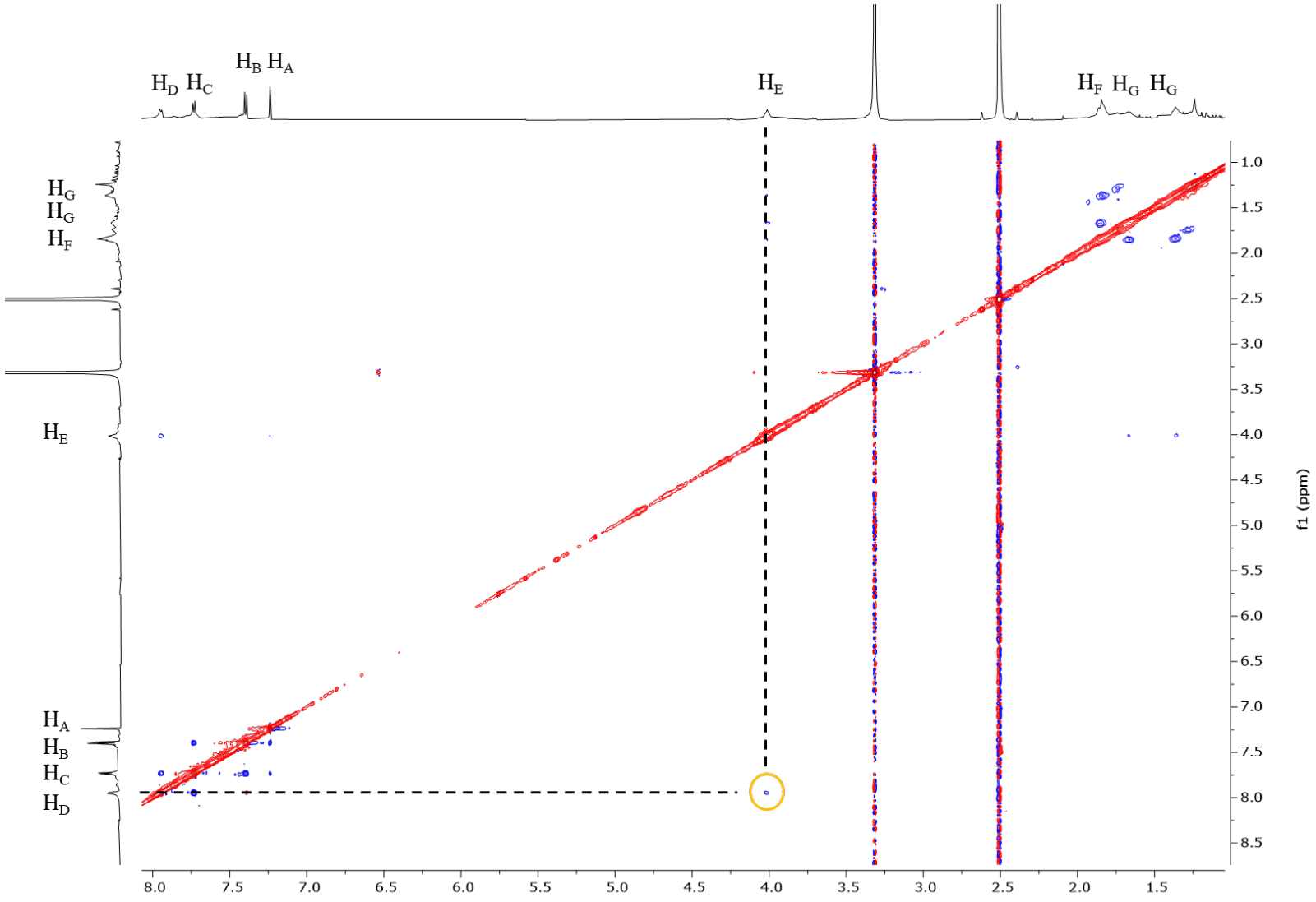
H_D H_C
H_B H_A
H_E
H_F H_G H_G
H_G
H_G
H_F
H_E
H_A
H_B
H_C
H_D
8.0 7.5 7.0 6.5 6.0 5.5 5.0 4.5 4.0 3.5 3.0 2.5 2.0 1.5
1.0 1.5 2.0 2.5 3.0 3.5 4.0 4.5 5.0 5.5 6.0 6.5 7.0 7.5 8.0 8.5
f1 (ppm)

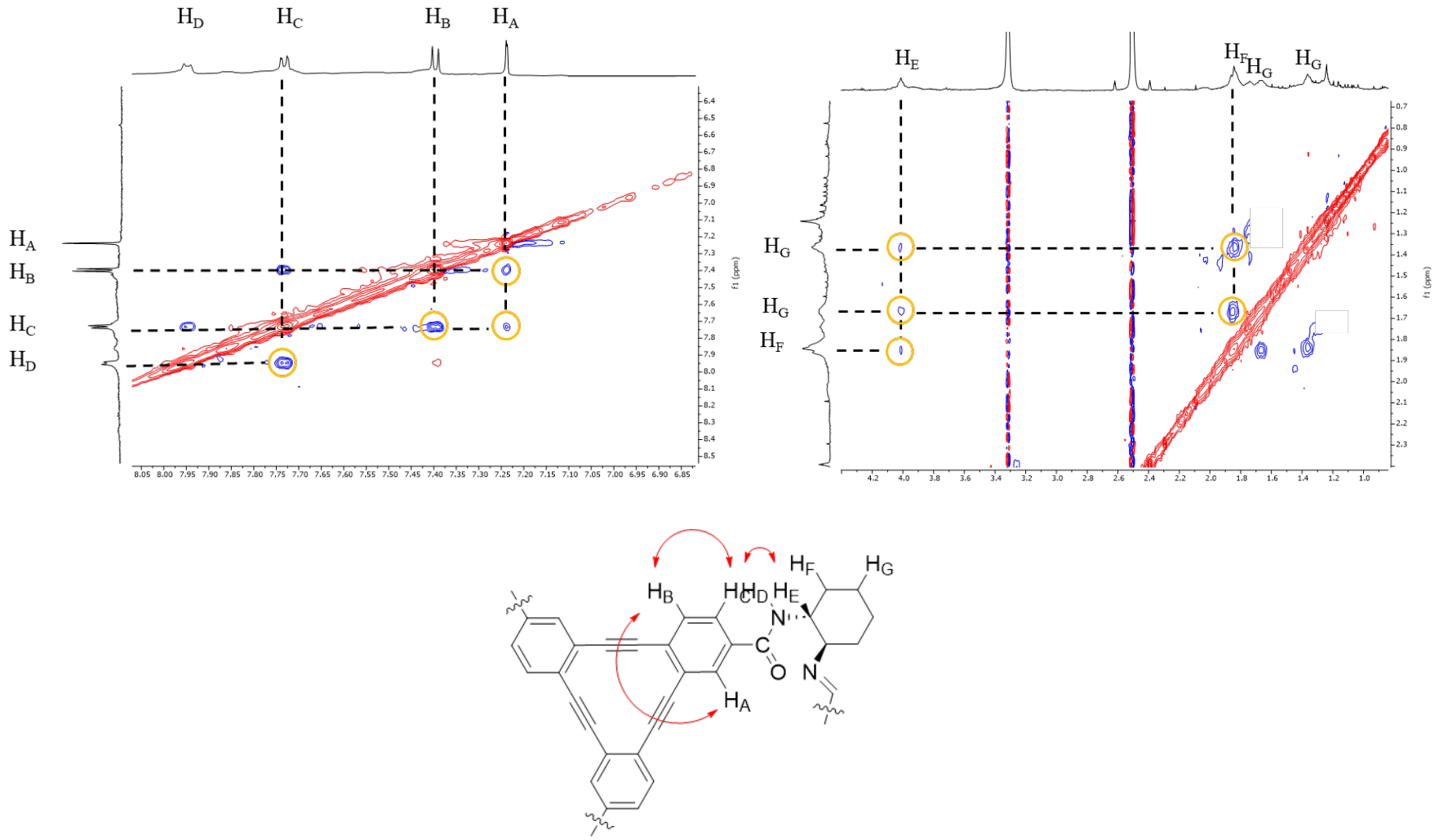

Figure S20. ^{1}H-^{1}H ROESY spectrum (600 MHz, 298K) of cage **5-*P*** in DMSO-d_6.

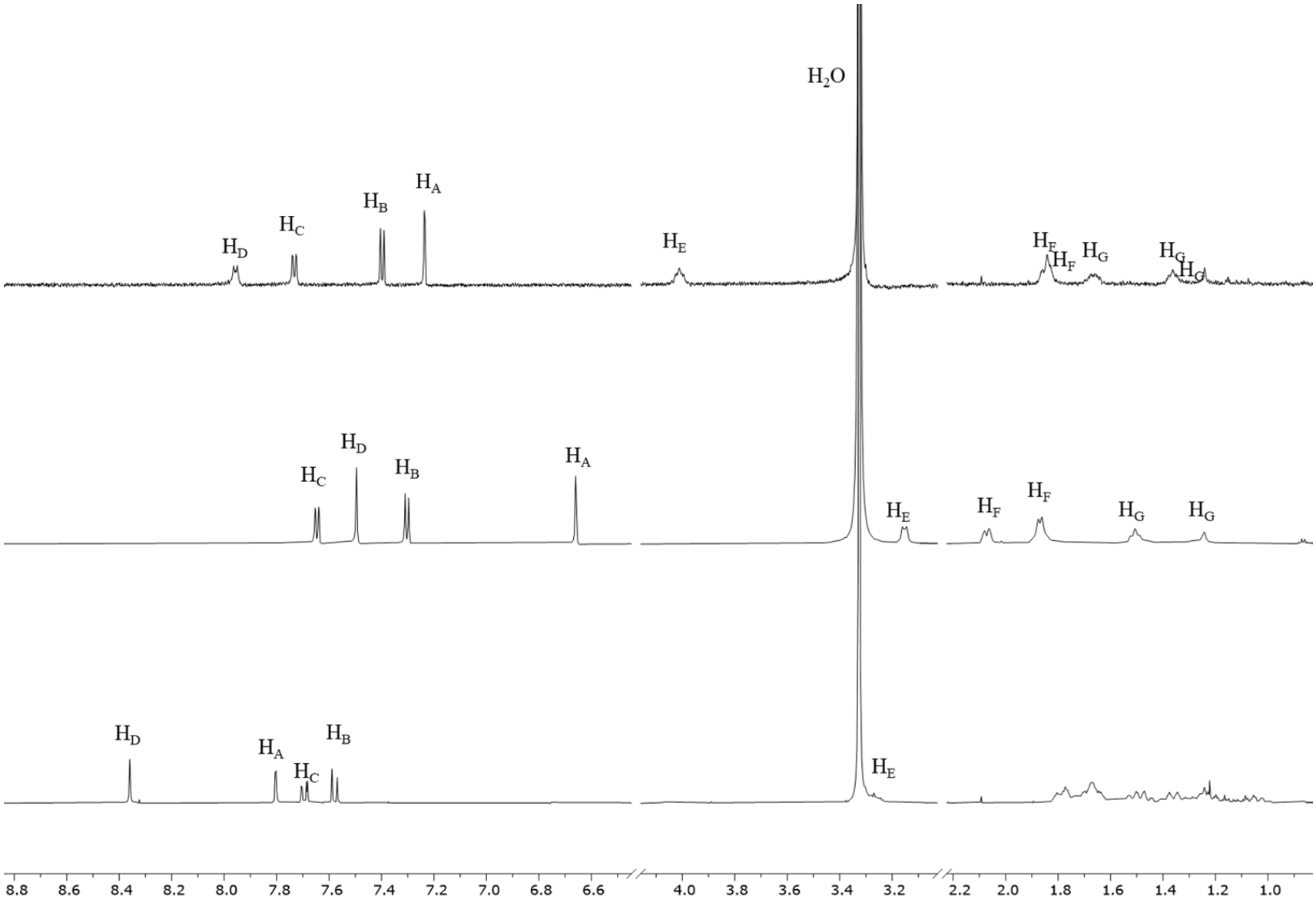

Figure S21. [1]H NMR spectra (600 MHz, 298K) of model compound **4** (bottom), imine cage **1**-*P* (middle), and amide cage **5**-*P* (top) in DMSO-d_6.

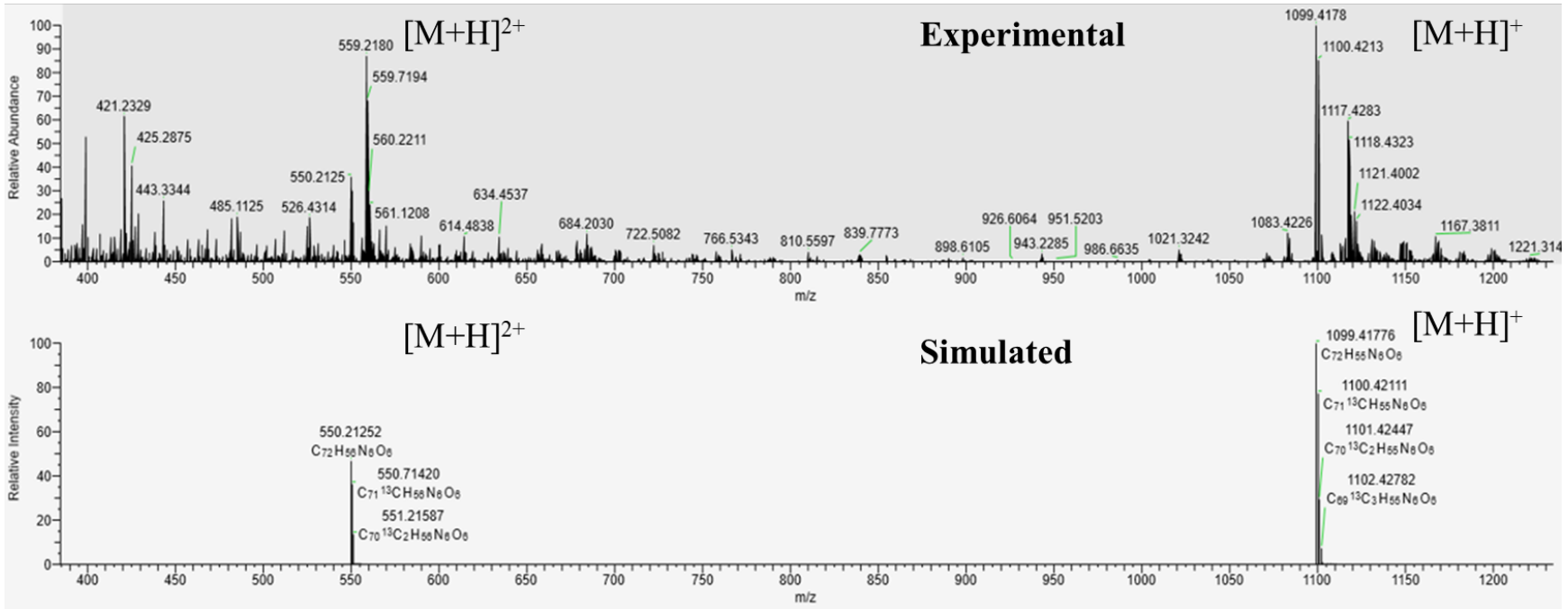

Figure S22. ESI-MS (Thermo Orbitrap) data of **5**-*P*, with experimental (top) and simulated (bottom) peaks. The mass of the labeled ions (singly and doubly charged) along with their isotope distribution (top) match the simulated mass of ions from **5**-*P*.

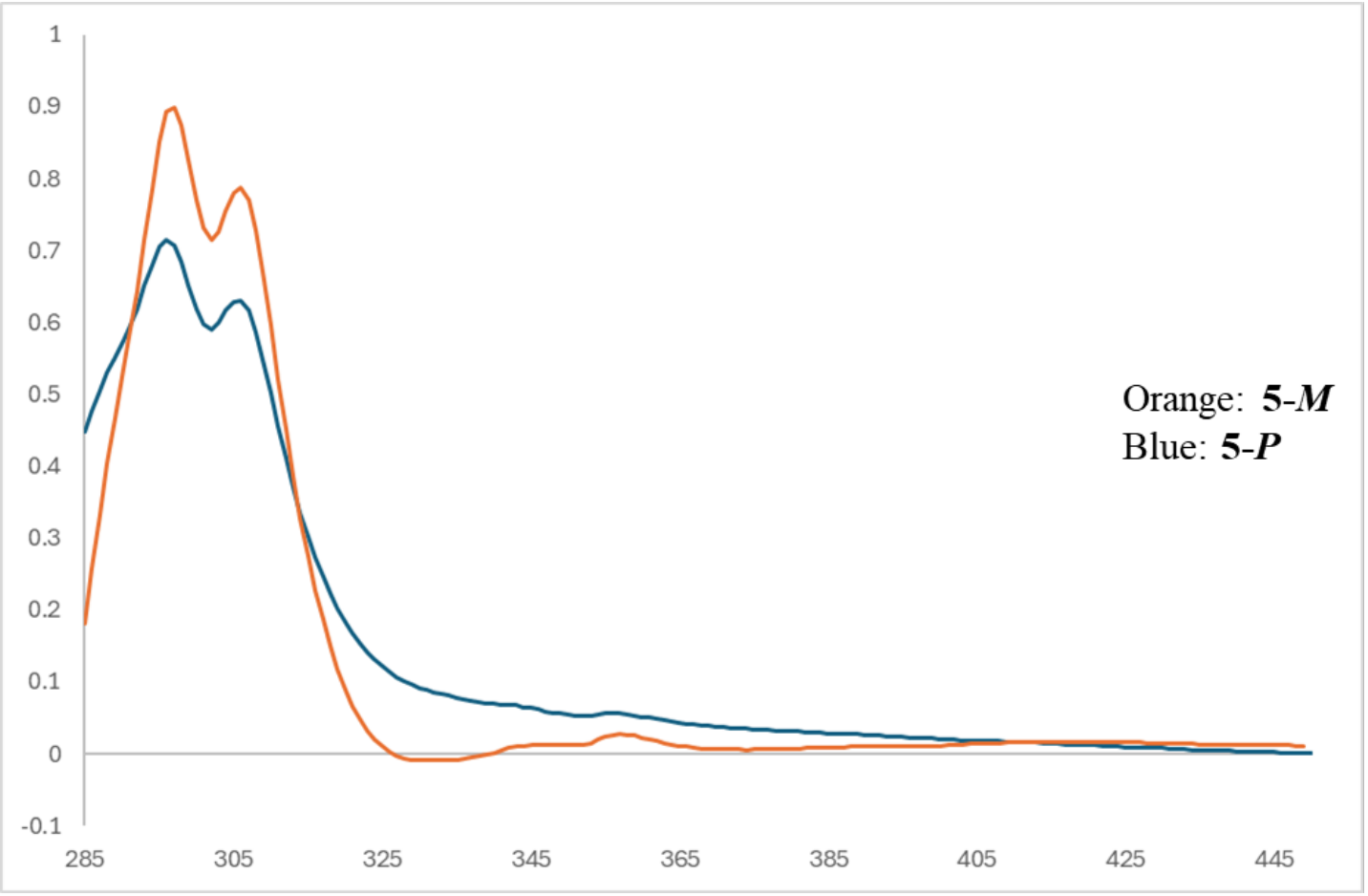

Figure S23. UV-Vis spectra of 55 µM solution of **5-*P*** (orange) and 45 µM solution of **5-*M*** (blue) in tetrahydrofuran. The presence of impurities (not easily detectable by ^{1}H NMR spectroscopy) could have affected the spectra at lower wavelengths.

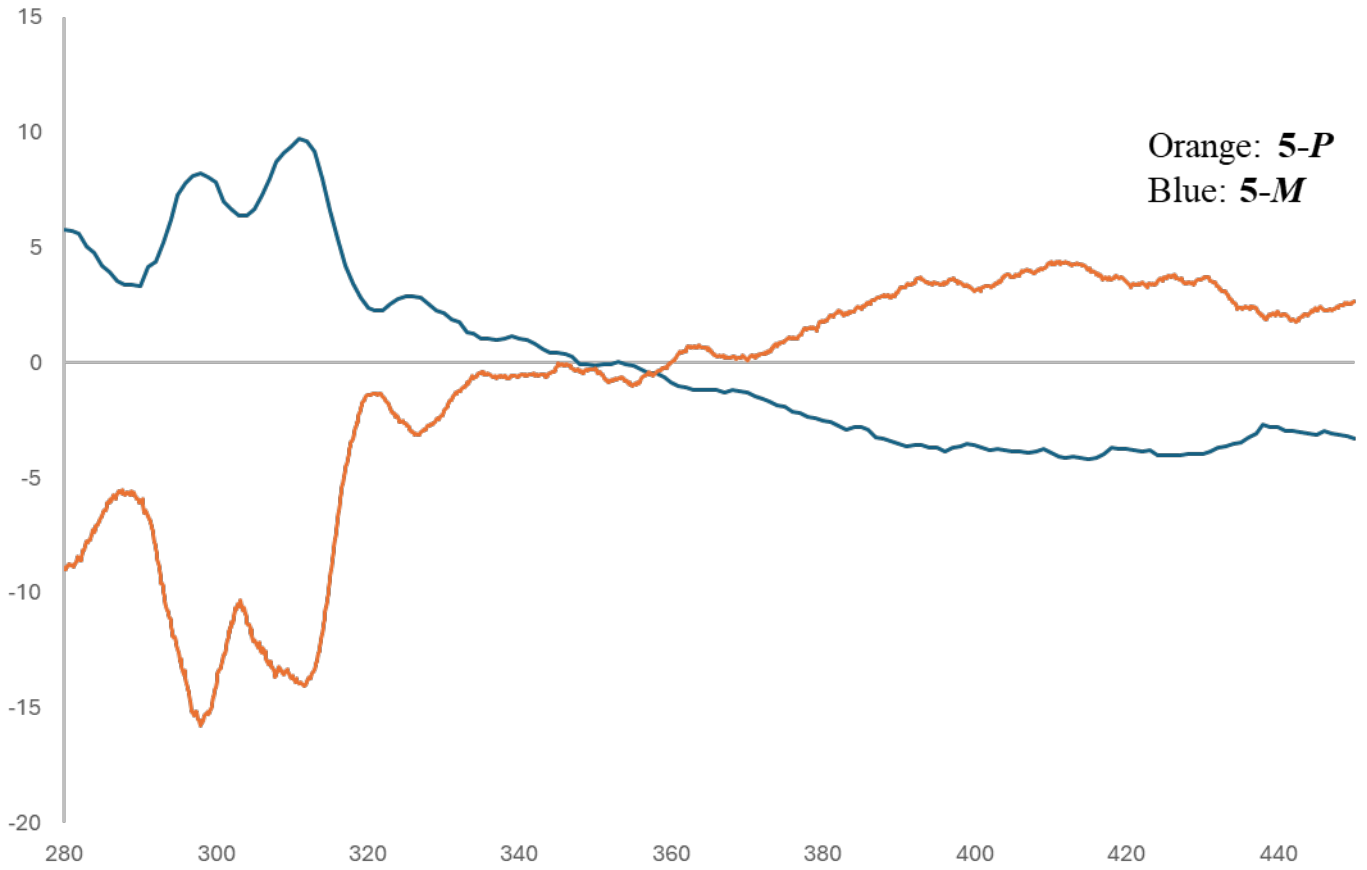

Figure S24. Circular dichroism (CD) spectra of 25 μM solution of **5-*P*** (orange) and 18 μM solution of **5-*M*** (blue) in tetrahydrofuran.

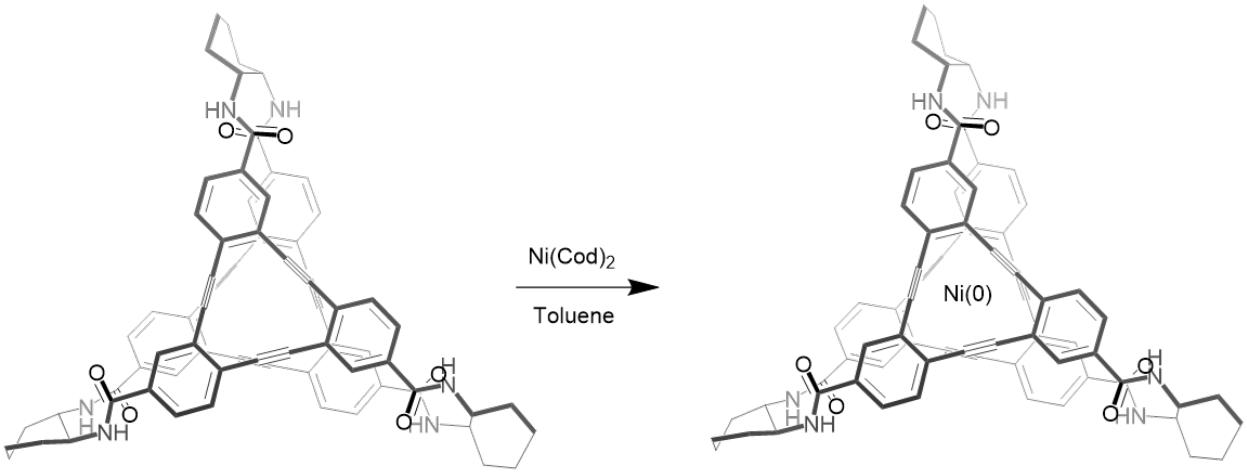

5-*P* [Ni(0)-5-*P*]

Scheme S6. A scheme showing Ni(0) metalation of **5-*P*** into [Ni(0)⊂**5**-*P*]. The procedure was completed inside an argon glovebox with the use of flame dried glassware and ahydrous/degassed solvents. $Ni(COD)_2$ (1.25 mg, 4.55 μmol) was added to a solution of **5**-*P* (5 mg, 4.55 μmol) in toluene (2 mL) followed by stirring for 16 h. The resulting suspension changed from yellow to dark blue during this time. Next, 2 mL of hexanes was added leading to precipitation. The precipitate was collected by vacuum filtration and washed with hexanes (~10 mL) to yield a dark blue solid material.

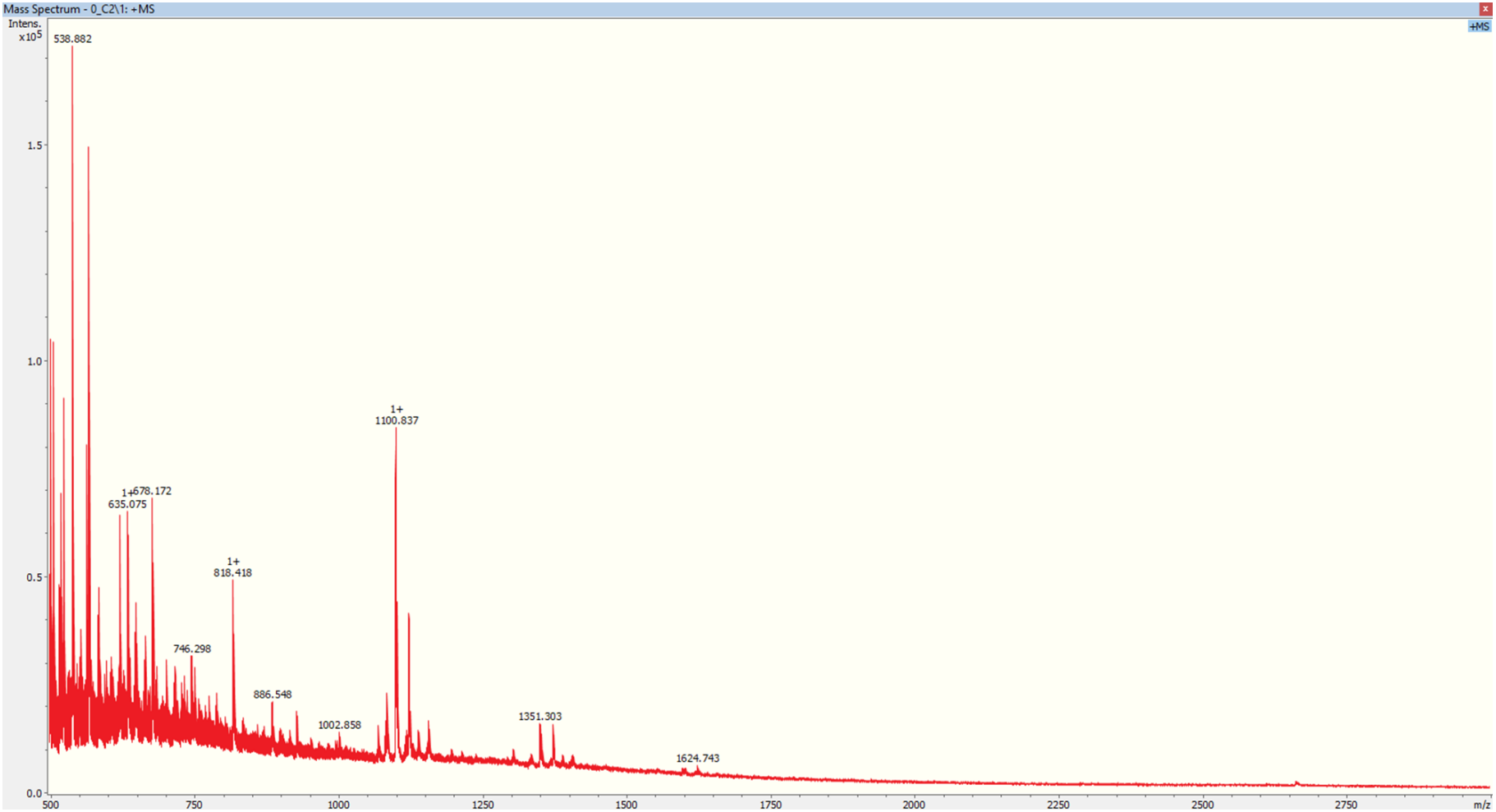
Mass Spectrum - 0_C2\1: +MS
Intens.
x10^5
+MS
538.882
1+
635.075
1+678.172
1+
818.418
746.298
886.548
1002.858
1+
1100.837
1351.303
1624.743
1.5
1.0
0.5
0.0
500
750
1000
1250
1500
1750
2000
2250
2500
2750
m/z

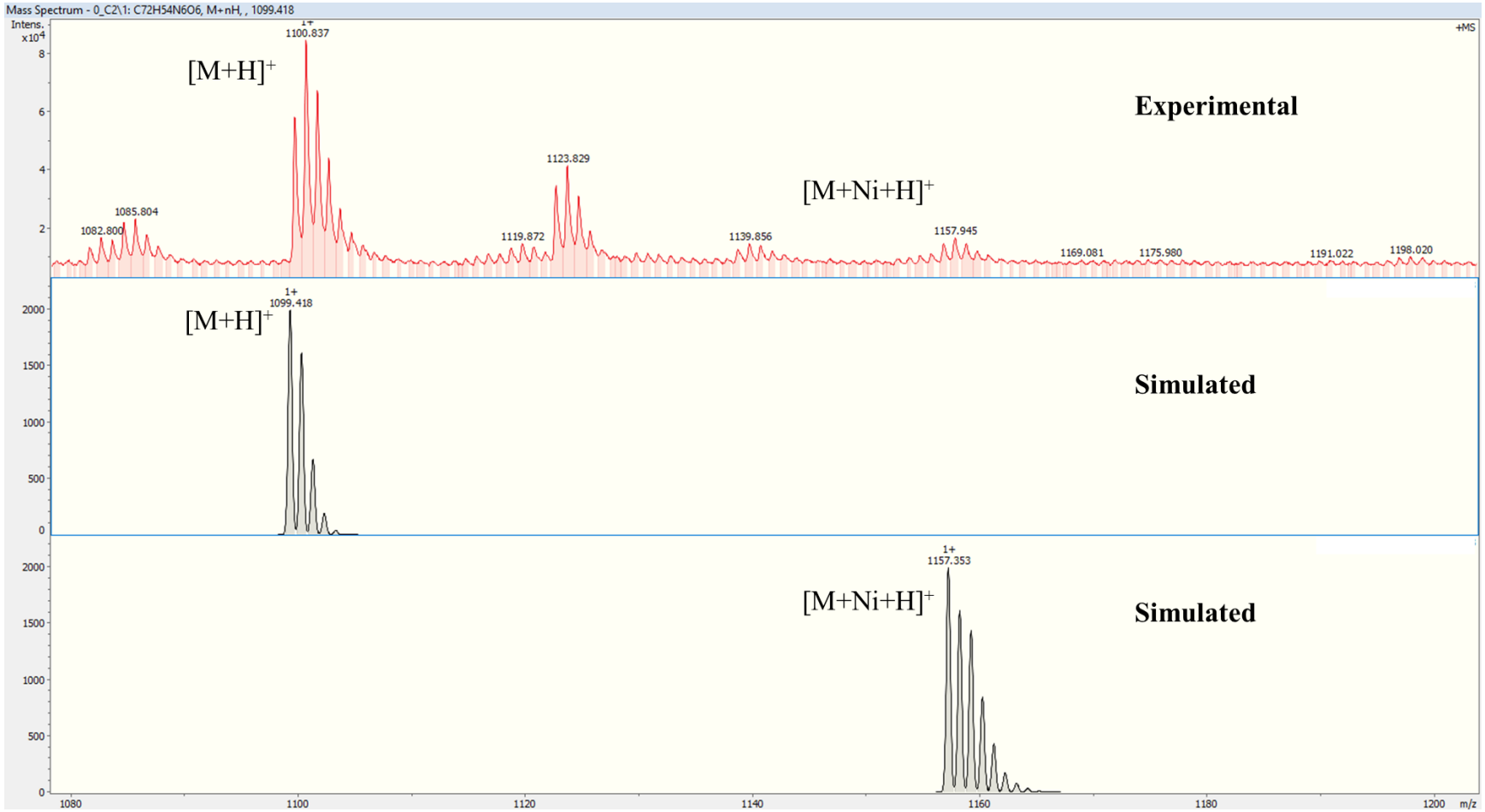

Figure S25. MALDI-TOF experimental data from a suspension of the solid product in Ni(0) metalation of **5**-*P* in tetrahydrofuran. An ion with the mass corresponding to [Ni(0)⊂**5**-*P*] is labeled.

Computational Methods

Organic cage **1**-*M* with (*S*,*S*) stereochemistry containing DBA moieties with imine linkages was subjected to geometry optimizations with Gaussian 16[1] and the 6-31+G* basis set (note, these calculations utilized the standard 6D cartesian *d* functions for these calculations).[2-5] Four different density functional theory (DFT) methods were applied, including the B3LYP,[6-9] B3LYP-D3,[6-10] CAM-B3LYP,[11] and ωB97XD[12] functionals, for the geometry optimizations of each basket. Due to the strong similarities between the structures obtained from B3LYP, CAM-B3LYP, and ωB97XD, only the B3LYP and B3LYP-D3 geometric structures were utilized for time-dependent density functional theory (TD-DFT) calculations for UV-vis evaluations. Each of these calculations were completed in the gas phase.

Using both the B3LYP/6-31+G* and the B3LYP-D3/6-31+G* optimized geometries of the ground states of **1**-*M*, a simulated UV-vis spectrum was computed in Gaussian 16 using the 6-31+G* basis set and the B3LYP, B3LYP-D3, CAM-B3LYP, and ωB97XD functionals. In each case, 50 excited states were calculated. The computed spectrum for the imine cage optimized through B3LYP-D3 before using ωB97XD for the TD-DFT calculation was further analyzed due to similarities to the experimental spectrum. The structure of **1-*M*** optimized at B3LYP-D3/6-31+G* is shown in **Figure S26**. An energy shift of -0.16 eV was performed on the computed UV-vis spectrum after comparison to the experimental results in THF. Through each TD-DFT calculation, a respective circular dichroism (CD) spectrum was calculated for the cage. Using the respective energy shifts from the UV-vis calculation, this spectrum was compared to the experimental CD spectrum taken in THF. The computed CD spectrum was used to determine which excited states contributed significantly to the excitonic coupling.

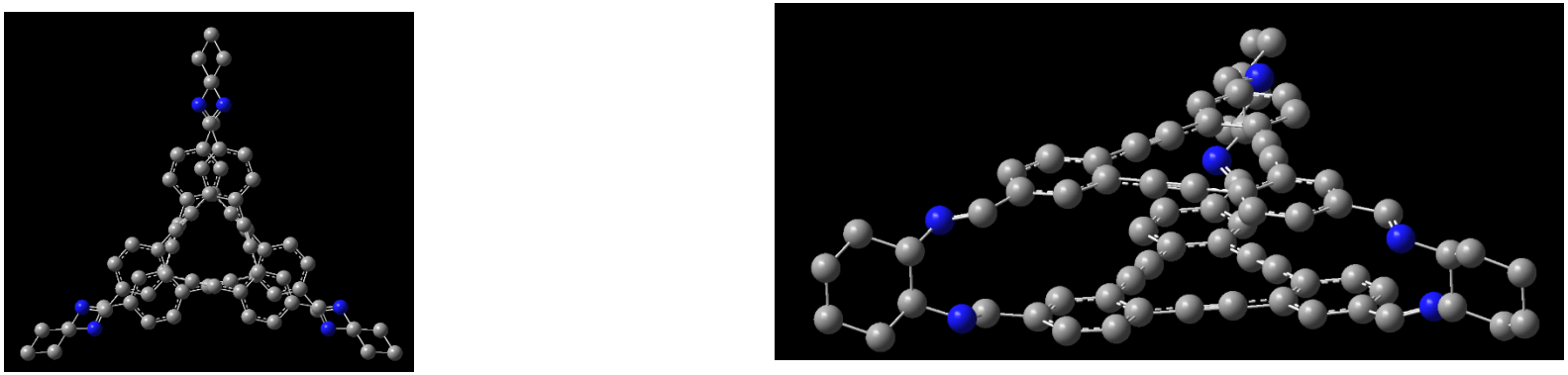

Figure S26. Structure of **1-*M*** optimized by B3LYP-D3/6-31+G*. Nitrogen atoms are colored dark blue and carbon atoms are colored grey. Note that all hydrogen atoms have been omitted for clarity.

a)

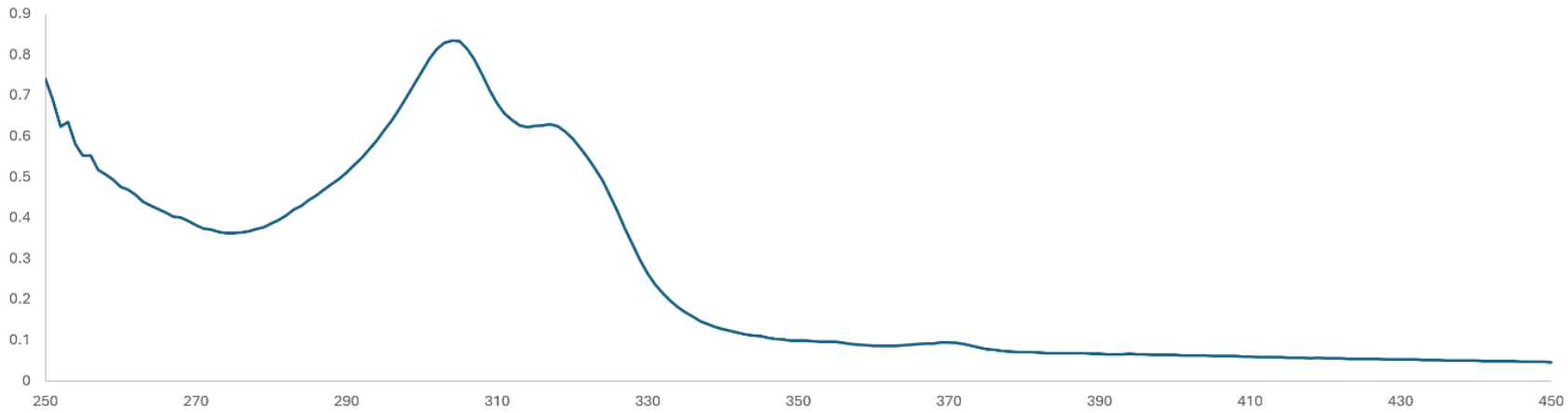
0.9
0.8
0.7
0.6
0.5
0.4
0.3
0.2
0.1
0
250
270
290
310
330
350
370
390
410
430
450

b)

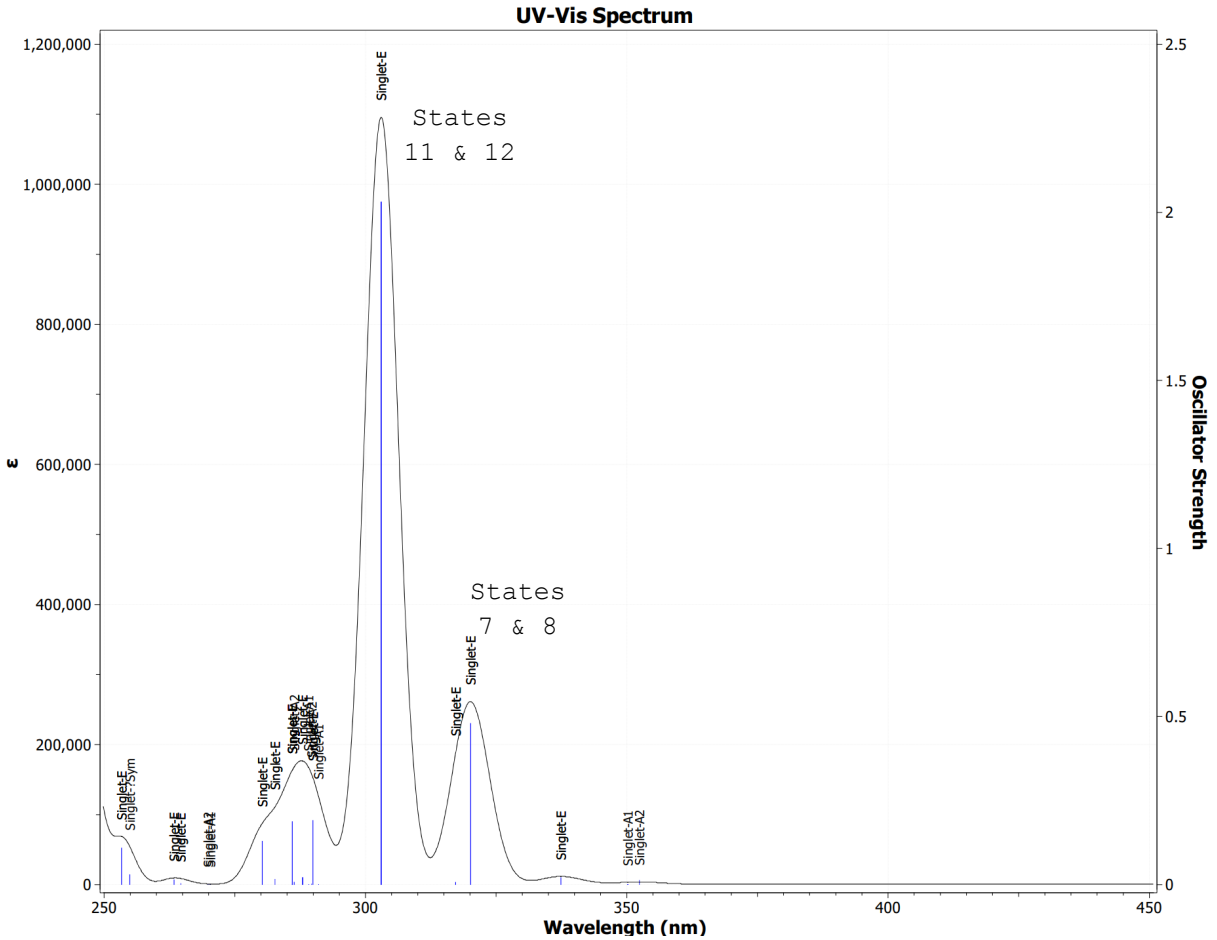

Figure S27. (a) Experimental UV-vis spectrum for **1-*M*** in THF. (b) Computed UV-vis spectrum for **1-*M*.** A broadening function of 0.05 eV as the UV-vis peak half-width at half height was applied. The cage was optimized at the B3LYP-D3/6-31+G* level of theory and the spectrum was computed at the ωB97XD/6-31+G* level of theory. Excited states hypothesized to be involved in relevant transitions have been labelled.

a)

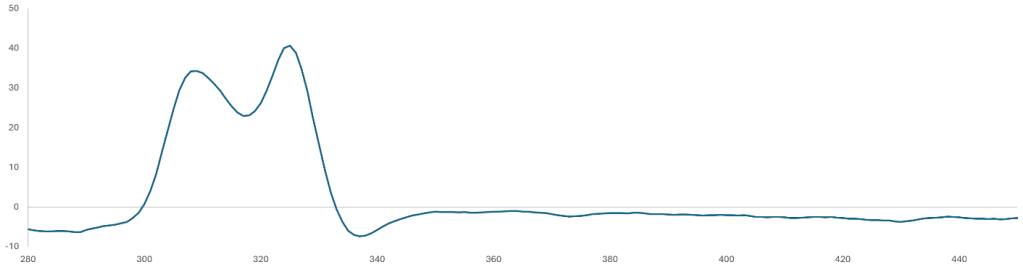

b)

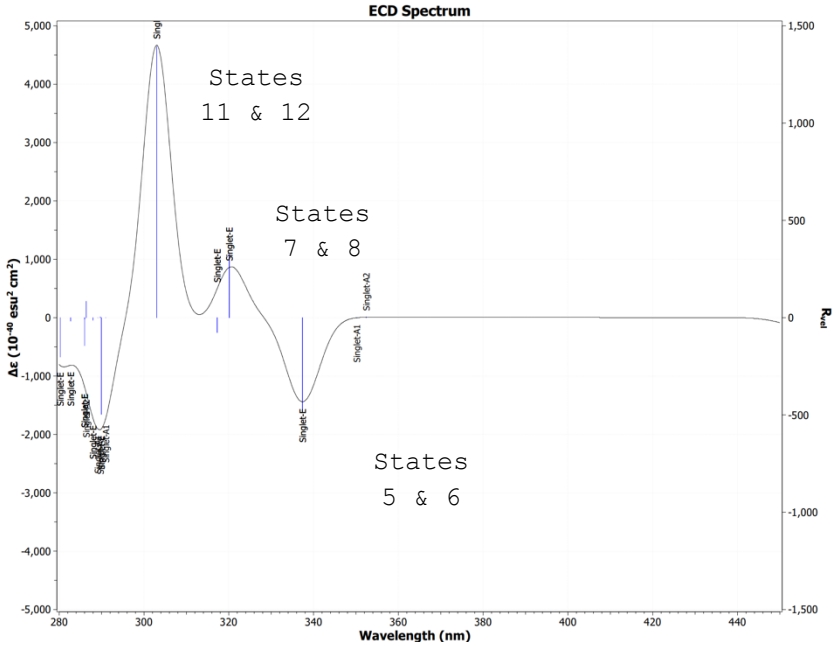

Figure S28. (a) Experimental CD spectrum for **1-*M*** in THF. b) Computed CD spectrum for **1-*M***, with (*S*,*S*) stereochemistry. A broadening function of 0.05 eV as the UV-vis peak half-width at half height was applied. The cage was optimized at the B3LYP-D3/6-31+G* level of theory and the spectrum was computed at the ωB97XD/6-31+G* level of theory. Excited states hypothesized to be involved in excitonic coupling have been labelled.

Figure S27: The computed UV-vis spectrum of compound **1-*M***. An energy shift was performed to match the highest-intensity peak with that of the experimental spectrum at 303 nm. Following the energy shift, the computed spectrum displayed an additional excited state of lower intensity at 320 nm. The experimental spectrum shows a similar peak at 317 nm, although it has a higher relative intensity compared to the peak at 303 nm. The experimental spectrum also displays a small, broad peak with a maximum absorbance at 370 nm; the computed spectrum shows a similar low-intensity excited state at 352 nm. Despite some discrepancies between the computed and experimental spectra for this compound, the overall similarities between the two ultimately display a level of agreement between the two for this basket.

Figure S28: The experimental CD spectrum of compound **1-*M***. The computed spectrum shows two significant excited states above the x-axis, with the peak at 303 nm having a higher intensity than that at 312 nm. Similarly, the experimental spectrum shows two peaks above the x-axis, with a peak at 308 nm having a lower intensity than a peak at 325 nm. Additionally, the computed spectrum displays a peak below the x-axis at 337 nm; the experimental spectrum shows a peak below the x-axis at 336 nm. The nearly identical nature of this peak coupled with the similar trends of the additional peaks above the x-axis offer further computational evidence displaying the agreement between the experimental and TD-DFT results.

Noncovalent Interaction Plot

Cage 1-*M* was optimized in Gaussian 16 using B3LYP-D3/6-31+G* level of theory. A noncovalent interaction (NCI) plot was generated for the optimized structure in multiwfn (Lu, T. A Comprehensive Electron Wavefunction Analysis Toolbox for Chemists, Multiwfn. *J. Chem. Phys.,* 161, 082503 (2024). 10.1063/5.0216272 and Lu, T.; Chen, F. Multiwfn: A multifunctional wavefunction analyzer. *J. Comp. Chem.* 33, 580-592 (2012). 10.1002/jcc.22885) and visualized in PyMOL. Two views of the resulting plot are shown in **Figure S29**, with the green isosurface representing the noncovalent bonds. The centers of each benzene and cyclohexane moiety show regions of repulsions.

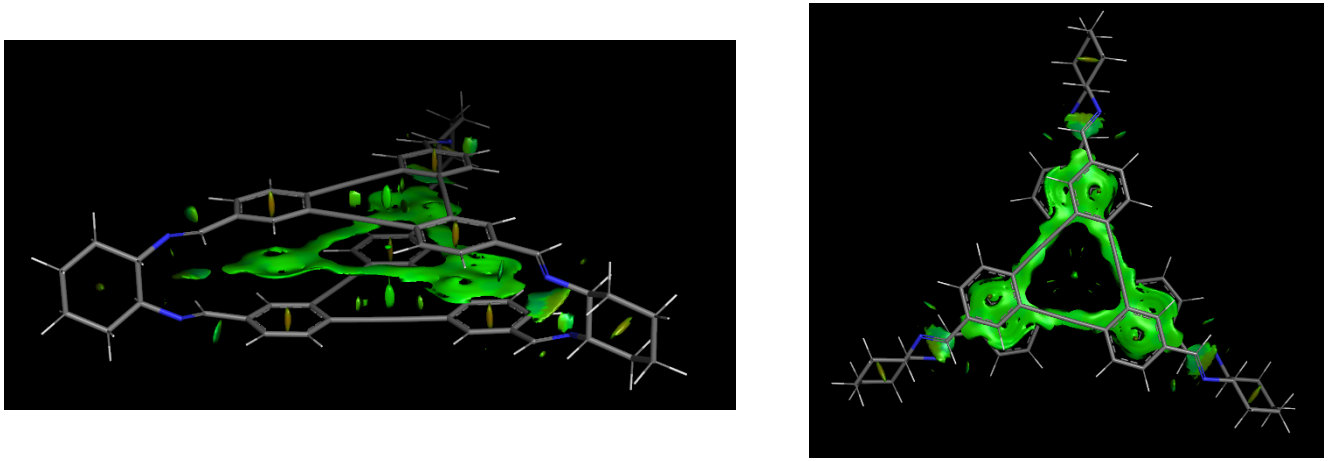

Figure S29. Noncovalent interaction plot (NCI) of **1-*M***, (B3LYP-D3/6-31+G*) with the green isosurface between the two DBA units depicting π–π noncovalent bonding.

Compound 1-*M*
B3LYP-D3/6-31+G*

Cartesian Coordinates

C	5.75081	-3.22612	1.53640
N	6.24656	-4.36720	1.24741
C	-5.66931	-3.36729	1.53640
N	-6.90539	-3.22608	1.24741
C	-0.08150	6.59341	1.53640
N	0.65883	7.59328	1.24741
C	5.66931	-3.36729	-1.53640
N	6.90539	-3.22608	-1.24741
C	-5.75081	-3.22612	-1.53640
N	-6.24656	-4.36720	-1.24741
C	0.08150	6.59341	-1.53640
N	-0.65883	7.59328	-1.24741
C	-0.66661	10.06151	-1.32210
C	0.01412	8.79509	-0.78580
C	-0.01412	8.79509	0.78580
C	0.66661	10.06151	1.32210
C	0.00572	11.33256	0.76834
C	-0.00572	11.33256	-0.76834
C	9.04682	-4.45345	-1.32210
C	7.60971	-4.40977	-0.78580
C	7.62383	-4.38532	0.78580
C	8.38021	-5.60805	1.32210
C	9.81143	-5.67123	0.76834
C	9.81715	-5.66133	-0.76834
C	-8.38021	-5.60805	-1.32210
C	-7.62383	-4.38532	-0.78580
C	-7.60971	-4.40977	0.78580
C	-9.04682	-4.45345	1.32210
C	-9.81715	-5.66133	0.76834
C	-9.81143	-5.67123	-0.76834
H	6.37790	-2.32046	1.55202
H	-5.19853	-4.36320	1.55202
H	-1.17938	6.68365	1.55202
H	5.19853	-4.36320	-1.55202
H	-6.37790	-2.32046	-1.55202
H	1.17938	6.68365	-1.55202
H	-1.72881	10.03294	-1.04208

H	-0.62832	10.04919	-2.41866
H	-1.07885	8.79950	1.08195
H	0.62832	10.04919	2.41866
H	1.72881	10.03294	1.04208
H	-1.02910	11.39555	1.13746
H	0.52825	12.22027	1.14699
H	1.02910	11.39555	-1.13746
H	-0.52825	12.22027	-1.14699
H	9.55318	-3.51928	-1.04208
H	9.01702	-4.48045	-2.41866
H	8.16001	-3.46544	1.08195
H	8.38870	-5.56874	2.41866
H	7.82438	-6.51366	1.04208
H	10.38339	-4.80655	1.13746
H	10.31893	-6.56761	1.14699
H	9.35429	-6.58900	-1.13746
H	10.84719	-5.65265	-1.14699
H	-7.82438	-6.51366	-1.04208
H	-8.38870	-5.56874	-2.41866
H	-7.08117	-5.33406	1.08195
H	-9.01702	-4.48045	2.41866
H	-9.55318	-3.51928	1.04208
H	-9.35429	-6.58900	1.13746
H	-10.84719	-5.65265	1.14699
H	-10.38339	-4.80655	-1.13746
H	-10.31893	-6.56761	-1.14699
H	1.07885	8.79950	-1.08195
H	7.08117	-5.33406	-1.08195
H	-8.16001	-3.46544	-1.08195
C	-4.73991	-2.24450	1.73201
C	-2.84362	-0.14706	1.80723
C	-3.37043	-2.52565	1.78305
C	-5.16240	-0.90222	1.73401
C	-4.22795	0.12386	1.77738
C	-2.40910	-1.50369	1.81244
H	-3.03019	-3.55740	1.75943
H	-6.22504	-0.68616	1.68228
H	-4.55332	1.16009	1.77434
C	-1.02522	-1.82627	1.82353
C	0.15995	-2.09906	1.81967
C	4.31375	-2.98263	1.73201

C	1.54917	-2.38912	1.80723
C	3.36255	-4.01965	1.73401
C	3.87249	-1.65606	1.78305
C	2.50678	-1.33450	1.81244
C	2.00671	-3.72345	1.77738
H	3.70675	-5.04796	1.68228
H	4.59590	-0.84552	1.75943
H	1.27199	-4.52334	1.77434
C	-1.89782	0.91101	1.81967
C	-1.06899	1.80100	1.82353
C	0.42616	5.22714	1.73201
C	1.29446	2.53618	1.80723
C	1.79985	4.92188	1.73401
C	-0.50206	4.18171	1.78305
C	-0.09768	2.83819	1.81244
C	2.22124	3.59959	1.77738
H	2.51829	5.73412	1.68228
H	-1.56570	4.40292	1.75943
H	3.28133	3.36324	1.77434
C	1.73787	1.18805	1.81967
C	2.09421	0.02527	1.82353
C	-4.31375	-2.98263	-1.73201
C	-1.54917	-2.38912	-1.80723
C	-3.87249	-1.65606	-1.78305
C	-3.36255	-4.01965	-1.73401
C	-2.00671	-3.72345	-1.77738
C	-2.50678	-1.33450	-1.81244
H	-4.59590	-0.84552	-1.75943
H	-3.70675	-5.04796	-1.68228
H	-1.27199	-4.52334	-1.77434
C	-2.09421	0.02527	-1.82353
C	-1.73787	1.18805	-1.81967
C	-0.15995	-2.09906	-1.81967
C	1.02522	-1.82627	-1.82353
C	-0.42616	5.22714	-1.73201
C	-1.29446	2.53618	-1.80723
C	0.50206	4.18171	-1.78305
C	-1.79985	4.92188	-1.73401
C	-2.22124	3.59959	-1.77738
C	0.09768	2.83819	-1.81244
H	1.56570	4.40292	-1.75943

H	-2.51829	5.73412	-1.68228
H	-3.28133	3.36324	-1.77434
C	4.73991	-2.24450	-1.73201
C	2.84362	-0.14706	-1.80723
C	5.16240	-0.90222	-1.73401
C	3.37043	-2.52565	-1.78305
C	2.40910	-1.50369	-1.81244
C	4.22795	0.12386	-1.77738
H	6.22504	-0.68616	-1.68228
H	3.03019	-3.55740	-1.75943
H	4.55332	1.16009	-1.77434
C	1.89782	0.91101	-1.81967
C	1.06899	1.80100	-1.82353

References

(1) Frisch G. W.; Schlegel, H. B.; Scuseria, G. E.; Robb, M. A.; Cheeseman, J. R.; Scalmani, G.; Barone, V.; Petersson, G. A.; Nakatsuji, H.; Li, X.; Caricato, M.; Marenich, A. V.; Bloino, J.; Janesko, B. G.; Gomperts, R.; Mennucci, B.; Hratch, D. J., M. J. . T. Gaussian 16, Rev. C.02. *Gaussian, Inc., Wallingford, CT* (2016).

(2) Clark, T.; Chandrasekhar, J.; Spitznagel, G. W.; Schleyer, P. V. R. Efficient Diffuse Function-Augmented Basis Sets for Anion Calculations. III. The 3-21+G Basis Set for First-Row Elements, Li-F. *J. Comp. Chem.* **4** (3), 294–301 (1983). 10.1002/jcc.540040303

(3) Ditchfield, R., Hehre, W. J., Pople, J. A. Self-Consistent Molecular-Orbital Methods. IX. An Extended Gaussian-Type Basis for Molecular-Orbital Studies of Organic Molecules. *J. Chem. Phys.* **54**, 724-728 (1971). 10.1063/1.1674902

(4) Hariharan, P. C.; Pople, J. A. The Influence of Polarization Functions on Molecular Orbital Hydrogenation Energies. *Theoret. Chim. Acta.* **28**, 213–222 (1973). 10.1007/bf00533485

(5) Hehre, W. J.; Ditchfield, R.; Pople, J. A. Self—Consistent Molecular Orbital Methods. XII. Further Extensions of Gaussian—Type Basis Sets for Use in Molecular Orbital Studies of Organic Molecules. *J. Chem. Phys.* **1972**, **56**, 2257–2261 (1972). 10.1063/1.1677527

(6) Becke, A. D. Density-Functional Thermochemistry. III. The Role of Exact Exchange. *J. Chem. Phys.* **98**, 5648–5652 (1993). 10.1063/1.464913

(7) Lee, C.; Yang, W.; Parr, R. G. Development of the Colle-Salvetti Correlation-Energy Formula into a Functional of the Electron Density. *Phys. Rev. B.* **37**, 785–789 (1988). 10.1103/physrevb.37.785

(8) Vosko, S. H.; Wilk, L.; Nusair, M. Accurate Spin-Dependent Electron Liquid Correlation Energies for Local Spin Density Calculations: A Critical Analysis. *Can. J. Phys.* **58**, 1200-1211 (1980). 10.1139/p80-159

(9) Stephens, P. J.; Devlin, F. J.; Chabalowski, C. F.; Frisch, M. J. Ab Initio Calculation of Vibrational Absorption and Circular Dichroism Spectra Using Density Functional Force Fields. *J. Phys. Chem.* **98**, 11623–11627 (1994). 10.1021/j100096a001

(10) Grimme, S. Semiempirical GGA-Type Density Functional Constructed with a Long-Range Dispersion Correction. *J. Comp. Chem.* **27**, 1787–1799 (2006). 10.1002/jcc.20495

(11) Yanai, T.; Tew, D. P.; Handy, N. C. A New Hybrid Exchange–Correlation Functional Using the Coulomb-Attenuating Method (CAM-B3LYP). *Chem. Phys. Lett.* **393**, 51–57 (2004). 10.1016/j.cplett.2004.06.011

(12) Chai, J.-D.; Head-Gordon, M. Long-Range Corrected Hybrid Density Functionals with Damped Atom–Atom Dispersion Corrections. *Phys. Chem. Chem. Phys.* **10**, 6615-6620 (2008). 10.1039/b810189b